https://doi.org/10.5194/essd-2021-209
Preprint. Discussion started: 24 June 2021

Open Access Earth System Science Data Discussions

VODCA2GPP - A new global, long-term (1988-2020) GPP dataset from microwave remote sensing

Benjamin Wild[1], Irene Teubner[1,2], Leander Moesinger[1], Ruxandra-Maria Zotta[1], Matthias Forkel[3], Robin van der Schalie[4], Stephen Sitch[5] and Wouter Arnoud Dorigo[1]

[1]Department of Geodesy and Geoinformation, TU Wien, Wiedner Hauptstraße 8, 1040 Vienna, Austria
[2]Zentralanstalt für Meteorologie und Geodynamik (ZAMG), Hohe Warte 38, 1190 Vienna, Austria
[3]Environmental Remote Sensing Group, Institute of Photogrammetry and Remote Sensing, Technische Universität Dresden, Helmholtzstraße 10, 01069 Dresden, Germany
[4]VanderSat, Wilhelminastraat 43A, 2011 VK Haarlem, the Netherlands
[5]College of Life and Environmental Sciences, University of Exeter, Exeter, EX4 4QE, UK

Correspondence to: Benjamin Wild (benjamin.wild@tuwien.ac.at)

Abstract. Long-term global monitoring of terrestrial Gross Primary Production (GPP) is crucial for assessing ecosystem response to global climate change. In recent years and decades, great advances in estimating GPP on a global level have been made and many global GPP datasets have been published. These global data records are either based on observations from optical remote sensing, are upscaled from in situ measurements, or rely on process-based models. The different estimation approaches are well established within the scientific community but also exhibit significant discrepancies among each other.

Here, we introduce the new VODCA2GPP dataset, which utilizes microwave remote sensing estimates of Vegetation Optical Depth (VOD) to estimate GPP on a global scale. VODCA2GPP is able to complement existing products with long-term GPP estimates covering the period 1988 - 2020. VODCA2GPP applies a previously developed carbon sink-driven approach (Teubner et al., 2019, 2021) to estimate GPP from the Vegetation Optical Depth Climate Archive (Zotta et al., in prep.; Moesinger et al., 2020), which merges VOD observations from multiple sensors into one long-running, coherent data record. VODCA2GPP was trained and evaluated against FLUXNET in situ observations of GPP and assessed against largely independent state-of-the art GPP datasets (MODIS GPP, FLUXCOM GPP, and GPP estimates from the TRENDY-v7 model ensemble).

These assessments show that VODCA2GPP exhibits very similar spatial patterns compared to existing GPP datasets across all biomes but with a consistent positive bias. In terms of temporal dynamics, a high agreement was found for regions outside the humid tropics, with median correlations around 0.75. Concerning anomalies from the long-term climatology, VODCA2GPP correlates well with MODIS and TRENDY-v7 GPP (Pearson's r: 0.53 and 0.61) but less with FLUXCOM GPP (Pearson's r: 0.29). A trend analysis for the period 1988-2019 did not exhibit a significant trend in VODCA2GPP on a global scale but rather suggests regionally differing long-term changes in GPP. Significant similar increases of global GPP that were found for VODCA2GPP, MODIS GPP, and the TRENDY-v7 ensemble for the shorter overlapping observation period (2003-2015)

https://doi.org/10.5194/essd-2021-209
Preprint. Discussion started: 24 June 2021

supports the theory of elevated CO_2 uptake potentially induced by increased atmospheric CO_2 concentrations and the associated rising temperatures.

The VODCA2GPP dataset is available at TU Data (https://doi.org/10.48436/1k7aj-bdz35; Wild et al., 2021).

1 Introduction

Gross Primary Production (GPP) describes vegetation's conversion of atmospheric CO_2 to carbohydrates through photosynthesis and it is the largest CO_2 flux in the carbon cycle (Beer et al., 2010). Estimates for the global mean annual GPP are ranging from 112 (Anav et al., 2015) up to 175 (Welp et al., 2011) petagrams of carbon per year. GPP is also considered the primary driver of the terrestrial carbon sink which is in total estimated to absorb approximately 30% of anthropogenic CO_2 emissions (Friedlingstein et al., 2020). GPP therefore plays a key role in mitigating the negative effects anthropogenic emission. Terrestrial vegetation productivity exhibits a high degree of (inter-)annual variability and evidence suggests that it is strongly affected by increasing concentrations of CO_2 in the atmosphere and the associated global climate change (Haverd et al., 2020; Schimel et al., 2015; Cox et al., 2000). Quantifying GPP is essential to understand the effect of climate variability and changes on the land carbon cycle (e.g., Baldocchi et al., 2016; Nemani et al., 2003).

Locally, GPP can be determined at in-situ flux towers, which measure the net exchange of carbon dioxide by means of eddy-covariances that are partitioned into GPP and ecosystem respiration (Baldocchi, 2003). FLUXNET (Pastorello et al., 2020) is the global network of regional flux tower networks (e.g., CarboAfrica, CarboItaly, etc.) to provide the scientific community with harmonized and well-documented flux observations. However, FLUXNET in-situ stations are sparsely and unevenly distributed across the planet, with most stations located in industrialized countries, which introduces a measurement bias and complicates the derivations of global ecosystem dynamics.

On the global scale, GPP is commonly estimated using optical remote sensing data in combination with (semi-)empirical or machine learning models (e.g., O'Sullivan et al., 2020; Jung et al., 2020; Gilabert et al., 2017; Alemohammad et al., 2017; Tramontana et al., 2016). Specifically, these models are based on light use efficiency (LUE) theory and/or statistical models that are applied to derive GPP based on optical remote sensing variables that are indicative of the vegetation's photosynthetic activity, such as the Fraction of Absorbed Photosynthetically Active Radiation (fAPAR), Leaf Area Index (LAI), vegetation indices, or Sun Induced Fluorescence (SIF). Optical remote sensing based datasets have the advantage of being available globally with high spatial resolution (usually in the order of 100 m to 1 km) and decent temporal resolution (e.g., 8-daily for MODIS). However, optical remote sensing is strongly affected by cloud cover, leading to data gaps and high uncertainties in regions with frequent cloud cover and high production such as tropical forests. Additionally, in very productive regions methods based on optical remote sensing tend to underestimate GPP (Turner et al., 2006).

https://doi.org/10.5194/essd-2021-209
Preprint. Discussion started: 24 June 2021


Open Access Earth System Science Data Discussions

Compared to optical remote sensing, Vegetation Optical Depth (VOD) from microwave remote sensing is much less affected by weather conditions. VOD describes the vegetation's attenuation of radiation in the microwave domain, which is controlled by its water content, biomass, type and density (Jackson and Schmugge, 1991; Vreugdenhil et al., 2016). Thus, VOD has been intensively used as proxy for above-ground biomass (Li et al., 2021; Rodríguez-Fernández et al., 2018; Tian et al., 2016; Liu et al., 2015) and is becoming increasingly important in the monitoring of vegetation dynamics (e.g., Frappart et al., 2020; Piles et al., 2017).

Recent studies investigated how GPP can be estimated from VOD (Teubner et al. 2018, 2019, 2021). GPP is significantly correlated with spatial patterns and temporal changes in VOD (Teubner et al., 2018). Based on this relationship, Teubner et al. (2019) developed a theoretical framework and a machine-learning method using FLUXNET observations to predict GPP using VOD. They showed that GPP can be adequately estimated for most regions of the world with an overall tendency for moderate overestimation and good temporal agreement with existing GPP products, especially for temperate regions. Recently, Teubner et al. (2021) improved this method by adding air-temperature in their model to account for temperature dependency of plant respiration, and found that this significantly improved the temporal agreement with reference GPP data.

However, until recently, long-term analysis of GPP from VOD was complicated due to relatively short observation periods of individual passive microwave remote sensing sensors (Moesinger et al., 2020). Moesinger et al. (2020) overcame this issue by merging single-frequency VOD from various sensors into the long-running Vegetation Optical Depth Climate Archive (VODCA) which comprises VOD observations of more than 20 years for X-, and C-Band and more than 30 years for Ku-Band. A new version of VODCA (Zotta et al., in prep.) does not only combine single sensors from identical frequencies but also merges observations from different bands (X, C and Ku) into a single long-running multi-frequency VOD climate archive with improved quality.

Here, we generate, evaluate and describe a novel long-term GPP dataset by applying the approach by Teubner et al. (2019, 2021) to the VODCA dataset. This microwave-based GPP dataset can likely complement existing datasets from optical satellite observations as it is less affected by cloud coverage which enables a consistent long-term analysis of changes in global gross primary production.

https://doi.org/10.5194/essd-2021-209
Preprint. Discussion started: 24 June 2021

Open Access Earth System Science Data Discussions

2 Data

2.1 Input to the VODCA2GPP model

2.1.1 VODCA

The Vegetation Optical Depth Climate Archive (VODCA v1; Moesinger et al., 2020) was first published in 2020 and consisted of three single-frequency VOD products (Ku-, X- and C-band), covering the period from 1987-2017 (Ku-Band), 1997-2019 (X-Band), and 2002-2019 (C-band), respectively. For VODCA2GPP, we used an updated VODCA version (VODCA v2 CXKu; Zotta et al., in prep) that merges all bands in a single dataset to obtain increased spatial and temporal coverage and reduced random errors compared to VODCA v1. VODCA v2 CXKu utilizes observations from the same sensors and frequencies as VODCA v1 (Table 1) to generate a single long-running VOD multi-frequency time series. It merges 15 passive night-time VOD datasets retrieved from seven different sensors via the Land Parameter Retrieval Model (LPRM; Van der Schalie et al., 2017). LPRM is based on radiative transfer theory introduced by Mo et al. (1982) and uses forward modelling to simulate the top of atmosphere brightness temperatures under a wide range of conditions and compares this to the actual satellite observation. Although primarily developed for soil moisture, it simultaneously solves for the VOD using an analytical solution by Meesters et al. (2005), utilizing the ratio between H and V polarized observations (Van der Schalie et al., 2017). LPRM requires that the soil and vegetation temperatures are equal, which may not be the case during the day due to uneven heating from solar radiation. VODCA v2 therefore uses only night-time observations which are assumed to have thermal equilibrium (Owe et al., 2008). Scaling of the single-sensor VOD observations is done by means of cumulative distribution function (CDF) matching (Moesinger et al., 2020).

Table 1: Input data for the used merged-band VODCA v2 with the main sensor specifications: used time periods, local ascending equatorial crossing times (AECT) and used frequencies. Table information is taken from Moesinger et al. (2020) and adapted for VODCA v2 CXKu.

Sensor	Time period used	AECT	C-Band [GHz]	X-Band [GHz]	Ku-Band [GHz]	reference
AMSR-E	Jun 2002 – Oct 2011	13:30	6.93	10.65	18.70	Van der Schalie et al. (2017)
AMSR2	Jul 2012 – Dec 2020 Jul 2012 – Aug 2017 (Ku-Band)	13:30	6.93, 7.30	10.65	18.70	Van der Schalie et al. (2017)
SSM/I F08	Jul 1987 – Dec 1991	18:15			19.35	Owe et al. (2008)
SSM/I F011	Dec 1991 – May 1995	17:00-18:15			19.35	Owe et al. (2008)
SSM/I F13	May 1995 – Apr 2009	17:45 – 18:40			19.35	Owe et al. (2008)
TMI	Dec 1997 – Apr 2015	Asynchronous		10.65	19.35	Owe et al. (2008); Van der Schalie et al. (2017)
WindSat	Feb 2003 – Jul 2012	18:00	6.80	10.70	18.70	Owe et al. (2008); Van der Schalie et al. (2017)

The preprocessing of LPRM level 2 VOD data used in VODCA v2 follows the steps described in detail in Moesinger et al. (2020). These include projecting the data into a 0.25° × 0.25° grid, using nearest neighbour resampling, selecting the closest

https://doi.org/10.5194/essd-2021-209
Preprint. Discussion started: 24 June 2021

night-time value in a window of ± 12 hours for every 0:00 UTC. The data are masked for radio-frequency interference (De Nijs et al., 2015), and negative VOD values and temperature. Different from Moesinger et al. (2020), masking for low land surface temperature (LST < 0°C), when the dielectric properties of water change drastically, is not based on Ka-band retrievals because these have high uncertainties over frozen land (Holmes et al. 2009). Instead, VODCA v2 uses the ERA-5 Land (Muñoz-Sabater et al. 2021) soil temperature level 1 (stl1) data. To ensure that all observations taken under frozen conditions are masked, all observations with an associated surface soil temperature (stl1) below 3°C are masked (Zotta et al., in prep.).

VODCA v2 CXKu is obtained by first scaling VODCA v2 observations from C- and Ku-band to X-band to remove systematic biases and then computing a weighted average in order to fuse overlapping observations. VODCA v2 CXKu provides a single, long-term vegetation metric covering over 30 years of observations (1988-2020) and thus exceeding the temporal length of the multi-sensor products (VODCA v2 C-, X and Ku). Due to the novel weighted averaging technique used in computing this dataset, the random error levels are lower, enabling the detection of long-term trends and dynamics at global scales (Zotta et al., in prep).

2.1.2 ERA5-Land – 2m Air Temperature

For representing the autotrophic respiration's temperature dependency 2 m air temperature (T2m) was derived from the ERA5-Land dataset. T2m is the most commonly used parameter for the describing the relationship between autotrophic respiration and temperature (Teubner et al., 2021; Drake et al., 2016; Ryan et al., 1997). ERA5-Land is a reanalysis dataset of meteorological variables which is provided by the European Centre for Medium-Range Weather Forecasts (ECMWF) (Muñoz-Sabater et al., 2021). ERA5-Land is produced at a spatial resolution of 8 km (~0.08°) and is available hourly.

2.1.3 FLUXNET2015 in-situ GPP

In-situ GPP data from Tier1 v1 FLUXNET2015 (Pastorello et al., 2020) was used to train and evaluate the VODCA2GPP product. FLUXNET GPP estimates are available for night-time and day-time flux partitioning, which were averaged as suggested by (Pastorello et al., 2020). FLUXNET data is available daily from 1991 until 2014 with a mean observation timespan of 7.27 ± 4.89 years for the used stations indicating significant variability in station data availability. An overview of the used FLUXNET2015 stations can be found in Table B1.

2.2 Reference datasets

2.2.1 MODIS GPP

GPP estimates derived from Moderate Resolution Imaging Spectroradiometer (MODIS) satellite data are based on Monteith's (1972) light-use efficiency concept which relates the amount of absorbed solar radiation to vegetation productivity. The MODIS algorithm uses fAPAR as proxy for the absorbed solar energy. For this study the MOD17A2H v006 GPP product was

https://doi.org/10.5194/essd-2021-209
Preprint. Discussion started: 24 June 2021

used (Running et al., 2015; Zhao et al., 2005). It is available at 8-daily temporal resolution and 500 m sampling and was resampled to 0.25° to match the resolution of VODCA2GPP.

2.2.2 FLUXCOM GPP

FLUXCOM GPP (Tramontana et al., 2016; Jung et al., 2020) is produced by upscaling GPP estimates from in-situ eddy covariances by means of various machine learning algorithms. Two FLUXCOM GPP setups exist: FLUXCOM RS uses high resolution land surface properties from MODIS observations as machine learning model input while FLUXCOM RS + METEO uses the mean seasonal cycle of land surface variables and additionally incorporates meteorological data (Jung et al., 2020). For validating VODCA2GPP, FLUXCOM RS was used because it includes temporal properties of land surface variables at finer spatial and temporal resolution than FLUXCOM RS+METEO. FLUXCOM RS GPP has 10 km sampling and is available every, 8 days, in accordance with the MODIS input data. The data were aggregated to 0.25° to match VODCA2GPP's resolution.

2.2.3 TRENDY-v7 GPP

Additionally to remote sensing-based datasets, GPP estimates from the reanalysis-driven TRENDY-v7 ensemble of 16 dynamic global vegetation models (DGVMs) were used as independent reference dataset (Le Quéré et al. 2018; Sitch et al. 2015). TRENDY-v7 simulations consider forcing effects of climate, land use and changes in atmospheric CO_2 concentrations on ecosystem's productivity over the period 1950-2017. The TRENDY-v7 ensemble consists of the following global vegetation models: CABLE-POP, CLASS-CTEM, CLM5.0, DLEM, ISAM, JSBACH, JULES, LPJ, LPJ-GUESS, LPX, OCN, ORCHIDEE, ORCHIDEE-CNP, SDGVM, SURFEX and VISIT. All models simulate monthly GPP and have a 1° x 1°grid. For the comparison with VODCA2GPP, all models were regridded to 0.25° using nearest neighbour resampling and the ensemble mean GPP of all available TRENDY-v7 models was computed.

3 Methods

3.1 VOD2GPP-model

VODCA2GPP is based on the carbon-sink driven GPP estimation approach (the VOD2GPP-model) introduced by Teubner et al. (2019, 2021). The VOD2GPP-model describes the theoretical relationship between GPP and VOD. The biogeochemical basis of this model is the relationship between GPP, the plant's net uptake of carbon (NPP) and autotrophic respiration (R_a) (Bonan, 2008):

$$GPP = R_a + NPP, \quad (3.1)$$

https://doi.org/10.5194/essd-2021-209
Preprint. Discussion started: 24 June 2021


Open Access Earth System Science Data Discussions

where Ra can be again split into two terms: maintenance respiration and growth respiration (Bonan, 2008). The VOD2GPP-model makes use of several VOD variables to represent the sum of NPP and Ra: the original VOD time series (VOD) which relates to maintenance respiration, temporal changes in VOD (Δ(VOD)) which relate to both growth respiration and NPP and the temporal median of VOD (mdn(VOD)) derived from the complete time series which serves as a proxy for the landcover. NPP is mostly represented by Δ(VOD) while Ra is represented by the original VOD signal and Δ(VOD). Thus, the VOD-based-only VOD2GPP-model can be formulated as follows (Teubner et al., 2019):

$$GPP(VOD) = s(VOD) + s(\Delta(\mathrm{VOD})) + s(mdn(VOD)), \quad (3.2)$$

where $s()$ denotes the mapping function that maps the input variables to GPP.

Eq. 3.2 represents a simplified model formulation that connects VOD to GPP but does not explicitly take into account the strong temperature dependency of aboveground vegetation's autotrophic respiration (Teubner et al., 2021; Wythers et al., 2013; Atkin et al., 2005; Tjoelker et al., 2001) which is mainly attributed to its maintenance part (Bonan, 2008; Ryan et al., 1997) . Therefore, an enhanced formulation of the model was developed by taking into account the temperature dependency of autotrophic maintenance respiration through a term representing the interaction between temperature (T2m) and VOD (Teubner et al., 2021):

$$GPP(VOD, T2m) = te(VOD, T2m) + s(\Delta(VOD)) + s(mdnVOD), \quad (3.3)$$

The mapping and interaction functions were implemented using generalized additive models (GAMs).

3.2 Generalized Additive Models

Generalized Additive Models (GAMs; Hastie and Tibshirani, 1990) are semi-parametric generalizations of linear models and combine properties of Generalized Linear Models (GLM) and additive models (Guisan et al., 2002). Link functions $f()$ are trained and summed up for each predictor in order to relate the expected value of a response variable $E(Y)$ to the explanatory variables x_i (Hastie and Tibshirani, 1990). The model can be written as:

$$E(Y) = \beta + \sum_{i=1}^{n} s_i(x_i), \quad (3.4)$$

where β denotes a constant offset and n corresponds to the number of input predictor variables x_i. The link functions $s_i()$ are implemented as smooth spline functions and allow the representation of non-monotonic and non-linear relationships which give them a high degree of flexibility (Hastie and Tibshirani, 1990). Hence, the relationship between target and predictor variables does not require explicit a-priori knowledge but can be estimated from the data itself, which makes GAMs appropriate

https://doi.org/10.5194/essd-2021-209
Preprint. Discussion started: 24 June 2021

for the VOD2GPP-model for which the exact relationship between VOD, air temperature, and GPP is difficult to determine (Teubner et al., 2019).

3.3 Preprocessing

The model-input data (FLUXNET GPP (response variable), VODCA v2 CXKu, ERA5-Land (predictor variables)) was resampled from daily to 8-daily resolution using the 8-day means over the respective time period in order to reduce noise and computation times. This means that also the final VODCA2GPP represents the mean of daily GPP for an 8-day period with an estimate every 8 days. Since VODCA v2 CXKu incorporates already extensive quality flagging (e.g., for temperature) no additional data cleansing was necessary.

For the computation of ΔVOD the resampled VOD observations were smoothed in order to increase the robustness of the derivation (Teubner et al., 2019). The smoothing was performed using a Savitzky-Golay filter with a window size of 11 data points as suggested by Teubner et al. (2021). ΔVOD was then obtained by subtracting the VOD observations at two consecutive timesteps. Median VOD ($mdnVOD$) was derived by computing the temporal median VOD of the entire time series for each available pixel.

3.4 Model training and output

For each valid FLUXNET2015 in-situ observation, the corresponding overlapping pixel values of VOD, ΔVOD, mdn(VOD) and T2m were gathered and used to set up the GAM. Data from days with one or more invalid or missing observations were not considered for model training. For training of the final VODCA2GPP model no data was retained as test data. The GAM-based implementation of the VOD2GPP-model is consistent with Teubner et al. (2021) and utilizes algorithms from the pygam python package (Servén et al., 2018).

The trained VODCA2GPP model was applied on each pixel where all input variables (VOD, ΔVOD, mdn(VOD) and T2m) were available. The result of this upscaling process is VODCA2GPP which covers the period between January 1988 and July 2020. Its spatial resolution is 0.25° and its temporal resolution is 8 days.

It is to be noted that with this approach it is in extreme cases also possible to obtain negative GPP values. Since negative GPP is not possible per definition, negative GPP estimates were set to zero in VODCA2GPP.

3.5 Uncertainty analysis

The robustness of the model was evaluated based on a uncertainty analysis during which the influence of the in-situ GPP station selection on the model was investigated. Specifically, the uncertainty was analysed by training 10 VODCA2GPP models with the proposed GAM approach while for each model run 10% of the station data was (pseudo-)randomly retained

https://doi.org/10.5194/essd-2021-209
Preprint. Discussion started: 24 June 2021


Open Access Earth System Science Data Discussions

(Teubner et al., 2019). This means that each of the 10 models was trained with 90% of the available FLUXNET stations. Every station was excluded exactly once which is why this approach is classified pseudo-randomly.

3.6 Product evaluation and assessment

For model evaluation, the 10 different model outputs from the uncertainty analysis were investigated by computing the minimum/maximum range as well as the standard deviation of the resulting 10 mean annual accumulated GPP estimates for each pixel. The standard deviation is also incorporated as uncertainty map in the available dataset (layer name: 'Uncertainties') to support users with an indicator for known uncertainties in VODCA2GPP.

Furthermore, annual GPP from VODCA2GPP, MODIS GPP and FLUXCOM GPP were evaluated against annual GPP from FLUXNET. The used error metrics were Root Mean Square Errors (RMSE) and Pearson's r. Global spatial GPP patterns were compared between the products by computing the mean annual GPP and the differences in mean annual GPP over the common observation period. Temporal agreements were tested by means of a Pearson correlation analysis for 8-daily GPP.

A correlation analysis of monthly GPP anomalies was conducted for all available datasets. Anomalies were derived by subtracting the long-term mean of the overlapping observation periods from 8-daily GPP estimates for each product.

Additionally, a trend analysis was conducted for all available GPP products in order to compare long-term changes in GPP. Trends in yearly median GPP were quantified using the Theil-Sen estimator (Theil, 1950; Sen, 1968) which calculates the slopes for each line between two point pairs. The median of all computed slopes is then used for line-fitting making it very insensitive to outliers and far more robust than simple linear regression (Wilcox, 2010). Slopes were considered as significant when then signs of the lower and upper 90%-confidence intervals were equal. For the trend analysis yearly median GPP was used.

https://doi.org/10.5194/essd-2021-209
Preprint. Discussion started: 24 June 2021

Open Access Earth System Science Data Discussions

4.1 Spatial patterns in global annual GPP

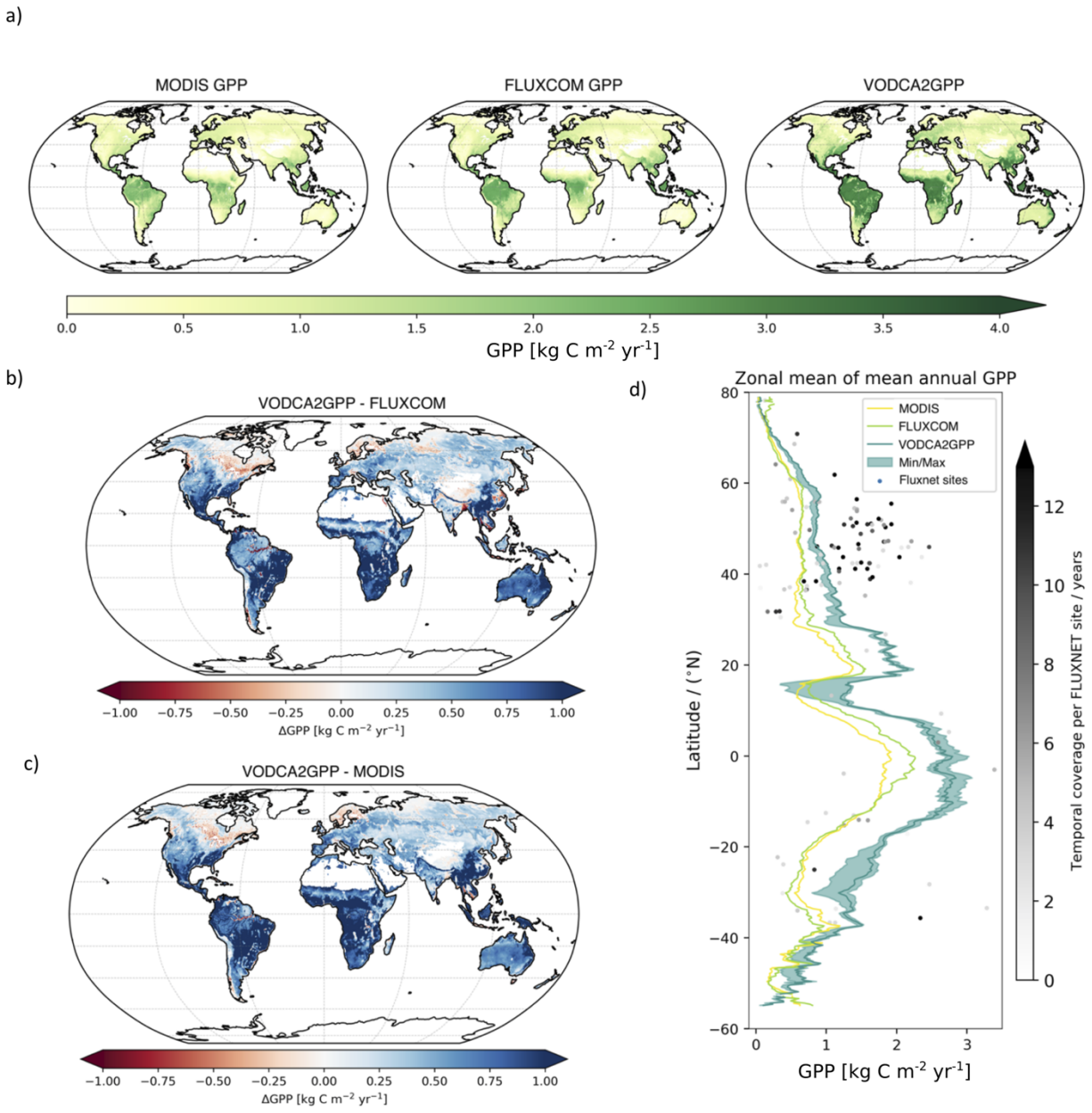

Figure 1: a) Mean yearly aggregated GPP for the common observation period of the three products (2002- 2016); b) and c) Difference in mean annual GPP between VODCA2GPP and the reference datasets; d) Latitude plot of zonal means of mean annual accumulated GPP. The means were computed based on 8-daily, 0.25 degree sampling. The Min/Max area denotes the minimum/maximum latitudinal mean for the ten model runs which were obtained during the uncertainty analysis. The dots represent the latitudinal location of the FLUXNET sites and the corresponding mean annual GPP. The brightness of the dots indicates the data availability for the respective FLUXNET station. Only data that is available in all three datasets was used for these plots.

https://doi.org/10.5194/essd-2021-209
Preprint. Discussion started: 24 June 2021

The average annual GPP of VODCA2GPP exhibits similar spatial patterns as the remote sensing-based references MODIS and FLUXCOM (Fig 1). The agreement in annual GPP is high in Northern latitudes (e.g., Europe, Russia, Canada) while there are relatively large differences in the southern hemisphere, especially in tropical regions (Fig 1d). The highest positive bias is observed in the subtropics. Very arid regions (e.g., Australian deserts, Kalahari Desert, etc.) have low mean yearly productivity in all three datasets (Fig 1a) but tend to be higher in VODCA2GPP compared to MODIS and FLUXCOM (Fig 1b, c). Comparison of the latitudinal distribution of FLUXNET station shows that lowest differences in yearly GPP are generally found in regions with high density of FLUXNET in-situ stations while largest bias is observed in regions with little or no FLUXNET coverage.

Similarly to the bias, uncertainties have a tendency to be smaller in latitudes with a high density of FLUXNET station (Fig 1d). The uncertainty map (Fig 2) shows that arid regions (e.g., Sahara, Australian deserts, Arabian Peninsula) as well as various mountainous regions (e.g., Carpathians, Alps, Rocky Mountains, Andes) have the highest model uncertainties (Fig 2). Moderate to high model instabilities are also exhibited for the tropics. Furthermore, significant uncertainties in VODCA2GPP are found in parts of Eastern and Western Siberia's boreal forests as well as in parts of Southern China.

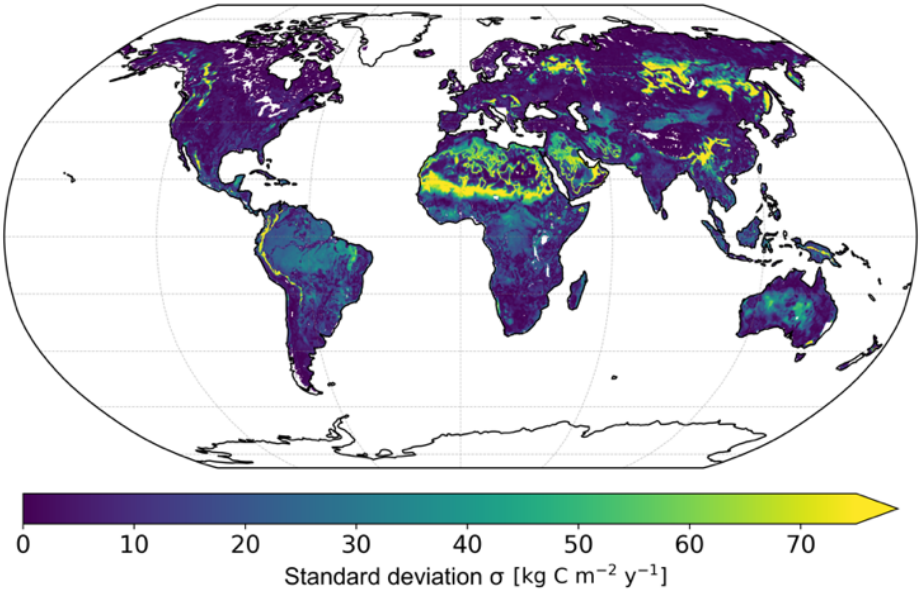

Figure 2: Standard deviation of mean yearly annual GPP (1988-2019) as obtained by the uncertainty analysis

VODCA2GPP's tendency towards a positive bias with respect to MODIS and FLUXCOM GPP products is not mirrored in the comparison against FLUXNET GPP. The in-situ comparison for MODIS and FLUXCOM GPP suggests a slight but systematic underestimation of GPP across all biomes (Fig 3). VODCA2GPP has a higher RMSE and lower Pearson's r than

https://doi.org/10.5194/essd-2021-209
Preprint. Discussion started: 24 June 2021

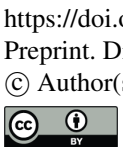

Open Access Earth System Science Data Discussions

the optical remote sensing based products indicating an overall slightly weaker performance. A landcover-based analysis (Fig A1) shows that uncertainties in annual VODCA2GPP are mostly occurring in (semi-)arid environments (e.g., savannas, open shrublands, grasslands). VODCA2GPP performs best in temperate environments (e.g., wetlands, evergreen broadleaf forest, croplands). Wetlands and evergreen broadleaf forests generally exhibit the best performance for all products while all three datasets underperform in open shrublands and deciduous broadleaf forest.

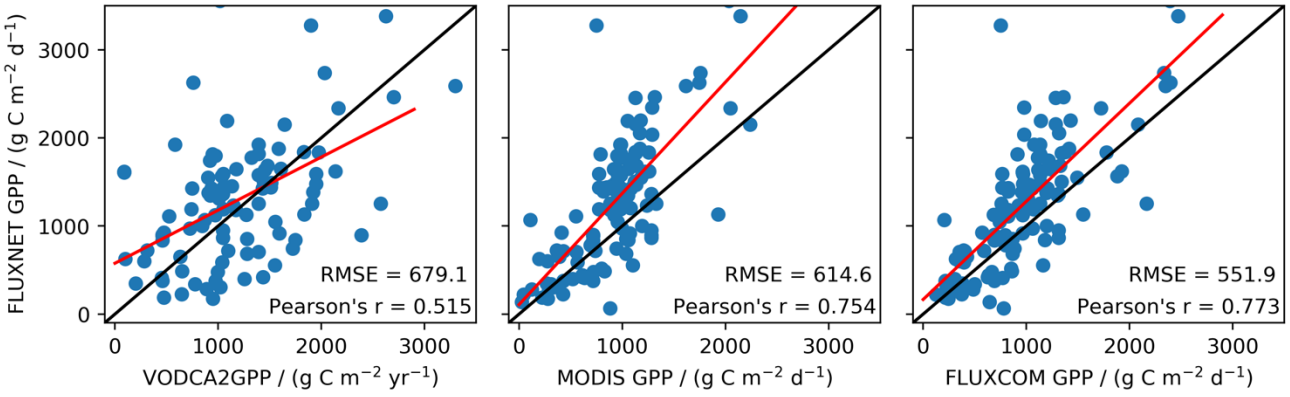

Figure 3: Mean annual in-situ GPP (FLUXNET) plotted against mean annual GPP from VODCA2GPP, FLUXCOM and MODIS for the respective grid cells. Mean annual GPP was computed from all available overlapping years and thus each station is represented by one dot. Red lines indicate the best linear fits determined by ordinary linear regression and the black lines represent the 1:1 lines.

4.2 Comparison of temporal dynamics

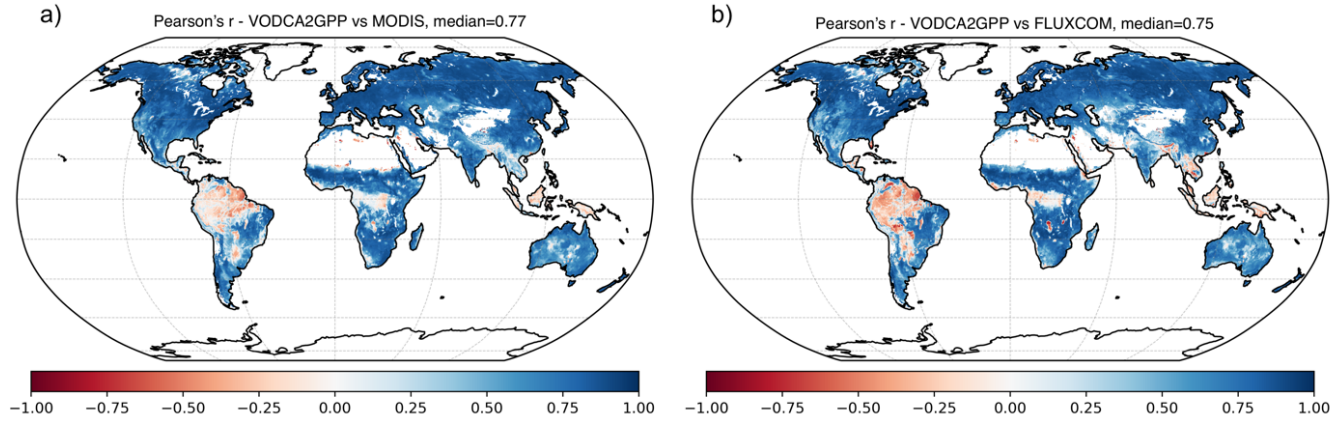

Figure 4: Pearson's r between VODCA2GPP and MODIS GPP (a) and VODCA2GPP and FLUXCOM GPP (b). The correlations are based on the common observation periods between 2002 and 2016 with 0.25° spatial and 8-daily temporal resolution.

https://doi.org/10.5194/essd-2021-209
Preprint. Discussion started: 24 June 2021

VODCA2GPP shows good temporal agreement with MODIS and FLUXCOM GPP. Pearson's r is highest in regions with distinct interannual variability such as sub-arctic, temperate, and semi-arid regions and lowest for dense tropical forests where partly even negative correlations occur (Fig 4). Median Pearson's r reaches 0.77 for MODIS GPP and 0.75 for FLUXCOM GPP.

4.3 Anomaly patterns in space and time

For a more detailed comparison of the products, monthly GPP anomalies were compared against each other. VODCA2GPP shows good correlation with MODIS and TRENDY-v7 GPP and weaker correlation with FLUXCOM GPP (Table 2, Fig 5). TRENDY-v7 correlates similarly well with VODCA2GPP and MODIS GPP and also shows worse correspondence with FLUXCOM GPP. The highest correlation is found between the two optical remote sensing based products MODIS and FLUXCOM GPP.

Table 2: Pearson's r correlation matrix for mean global monthly GPP anomalies between 2003 and 2016.

	VODCA2GPP	*MODIS GPP*	*FLUXCOM GPP*	*TRENDY-v7 GPP*
VODCA2GPP	1.00			
MODIS GPP	0.53	1.00		
FLUXCOM GPP	0.29	0.69	1.00	
TRENDY-v7 GPP	0.61	0.60	0.26	1.00

Analysis of the anomalies' temporal evolution and spatial distribution exhibits various similar patterns (Fig A2). Several extreme events are captured in VODCA2GPP and in at least one of the other GPP datasets. An example of such GPP extremes are the strong positive anomalies between 2010 and 2011 at around 25°S which were mainly caused by record-breaking rainfalls in Australia (Wardle et al., 2013). These positive anomalies are clearly visible in all examined GPP products apart from FLUXCOM which does not exhibit similarly striking patterns (Fig A2). Other GPP extremes that are noticeable in all products apart form FLUXCOM is extremely low GPP in 2002/2003 and early 2005 around 20°S (Fig A2). Both anomalies can be explained by extreme drought events that occurred in these years (Bureau of Meteorology, 2002/2003/2005; Horridge et al., 2005) which can be associated with El Niño events (Taschetto and England, 2009). Also, the distinct drop in GPP in 2015/2016 in similar latitudes might be linked to El Niño related drought events (Zhai et al., 2016). Generally, extreme events in VODCA2GPP are more pronounced than in the other datasets.

https://doi.org/10.5194/essd-2021-209
Preprint. Discussion started: 24 June 2021

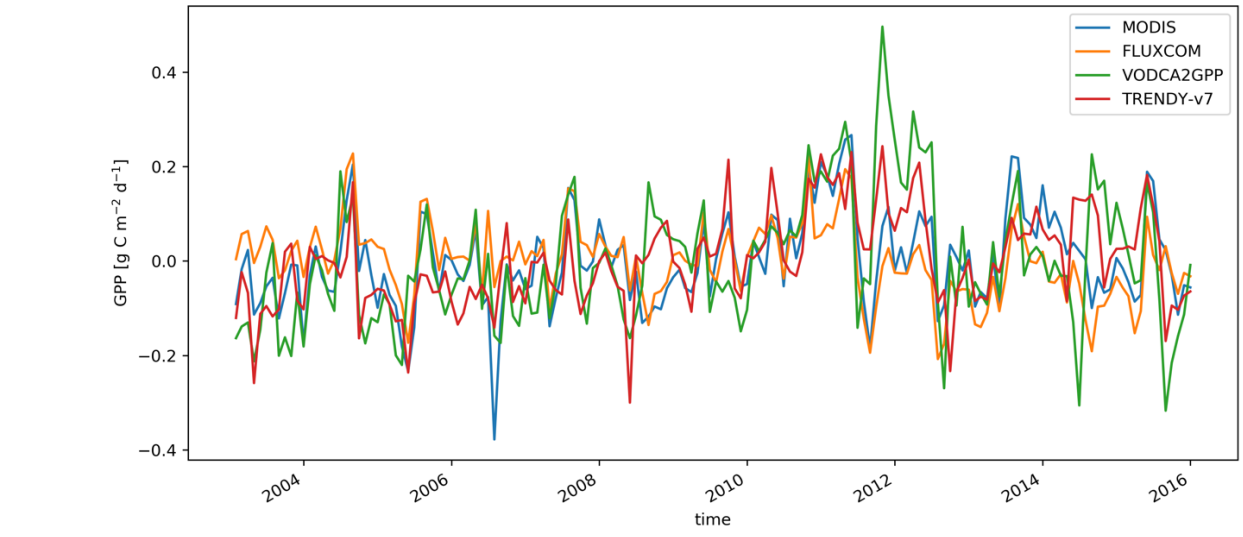

Figure 5: Time-series of mean global monthly GPP anomalies.

4.4 Global GPP trends

Trends in global annual median GPP between 2002 and 2016 are similar for VODCA2GPP, TRENDY-v7 GPP and MODIS GPP. All three products detect a significant increase of GPP during the observation period (Table 3, Fig 6). FLUXCOM GPP does not exhibit a significant trend but rather suggests a slight decrease in global annual median GPP.

The spatial distribution of GPP trends for the period 2003-2015 (Fig 7) exhibits many similarities between all analysed products. Large patterns of strong positive trends are, for example, found in Eastern parts of Siberia and China as well as in India and North America. Patterns of negative trends are found north of the Caspian Sea for all datasets. The remote sensing based products exhibit distinct patterns of declining GPP in central Siberia and significantly elevating GPP in Western Russia. Generally, the trends of VODCA2GPP match better with MODIS GPP and Trendy-v7 than with FLUXCOM. While there are many similar patterns on the Northern Hemisphere, trends on the Southern Hemisphere do not match well or are even contradictory. Especially in the Tropics hardly any similarities are visible.

For the full-time period (1988-2019) VODCA2GPP increases slightly on a global scale (Table 3), but this cannot be classified as significant due to contradictory upper and lower confidence intervals. The same is true for the slightly shorter period between 1988 and 2016 during which Trendy-v7 does detect a subtle significant trend on a global scale.

The spatial distribution of long-term (1988-2019; Fig 8) trends in VODCA2GPP is similar to the shorter period (2003-2015) but in general, long-term VODCA2GPP trends are less pronounced. The comparison of the fully overlapping period between VODCA2GPP and TRENDY-v7 (1988-2016, Fig A3) shows that TRENDY-v7 GPP exhibits weak but consistent positive

https://doi.org/10.5194/essd-2021-209
Preprint. Discussion started: 24 June 2021

trends for practically all biomes while VODCA2GPP trends are spatially strongly differing and for some regions even contradicting TRENDY-v7 trends.

A comprehensive comparison with in-situ GPP trends is hampered because most FLUXNET time series are too short to derive reliable trends. However, trends that were derived from available long-term time series (Fig A4) also suggest increasing GPP. Since this analysis is only based on very few stations this cannot be seen as evidence for positive GPP trends on a global scale.

Table 3: Theil-Sen trends in global yearly median GPP. Same signs of the upper/lower 90%-confidence interval indicate significant trends. The analysed periods are 2003-2015 which corresponds to the fully overlapping period for all datasets, 1989-2016 which corresponds to the fully overlapping period of VODCA2GPP and TRENDY-v7 and 1988-2019 which corresponds to all fully available years of VODCA2GPP.

	2003-2015		*1988-2016*		*1988-2019*	
	Theil-Sen slope [g C m-2 y-1]	Lower/Upper confidence interval	Theil-Sen slope [g C m-2 y-1]	Lower/Upper confidence interval	Theil-Sen slope [g C m-2 y-1]	Lower/Upper confidence interval
VODCA2GPP	0.013	+0.008 / +0.025	0.002	-0.001 / +0.006	0.002	-0.001 / +0.005
TRENDY-v7 GPP	0.017	+0.006 / +0.026	0.004	+0.000 / +0.008	-	-
MODIS GPP	0.012	+0.002 / +0.020	-	-	-	-
FLUXCOM GPP	-0.004	-0.009 / +0.001	-	-	-	-

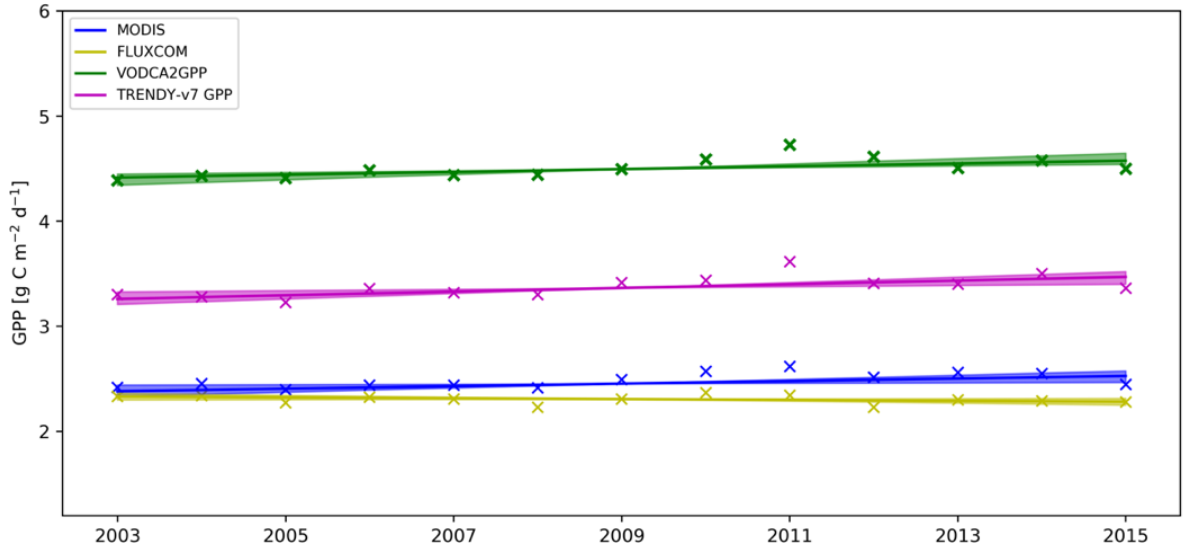

Figure 6: Time-series of yearly median GPP with the regression lines as obtained by the Theil-Sen estimator. Areas around the regression lines indicate the 90%-confidence intervals.

https://doi.org/10.5194/essd-2021-209
Preprint. Discussion started: 24 June 2021

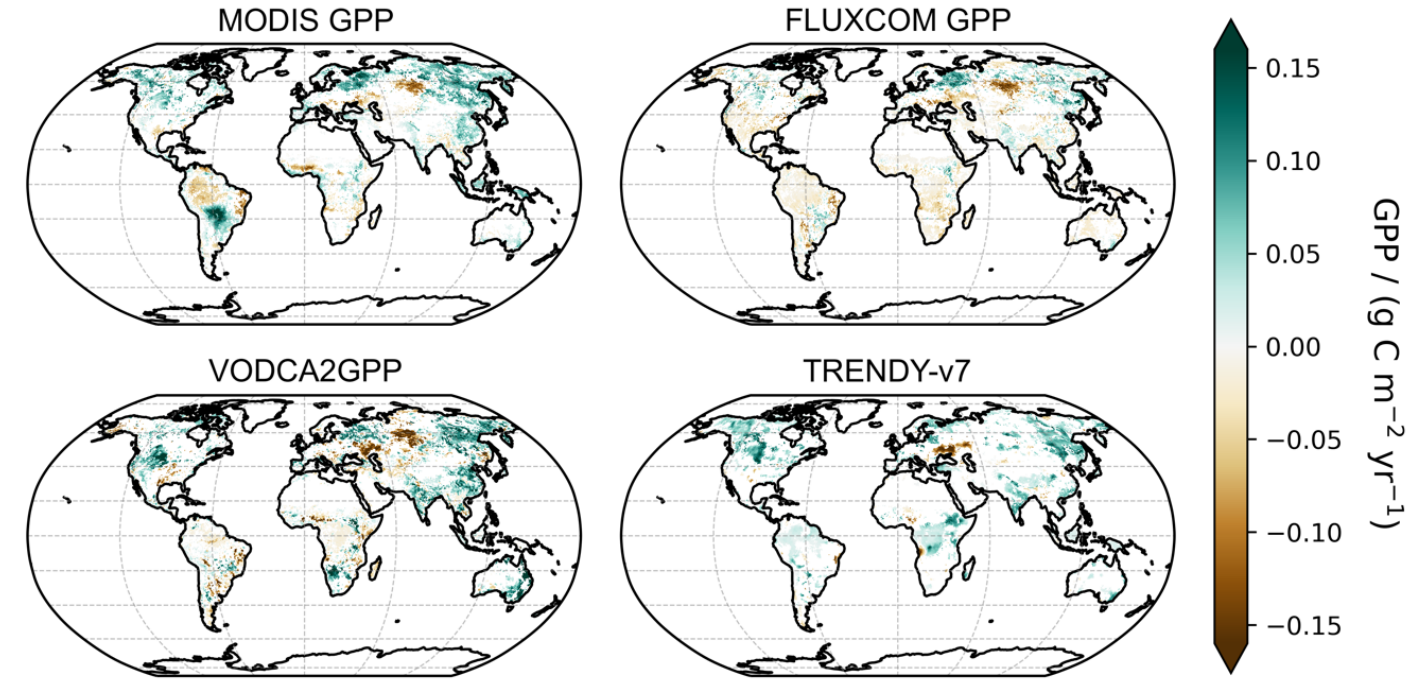

Figure 7: Global map of trends in yearly median GPP for the period 2003-2015 for all analysed datasets. White indicates non-significant trends.

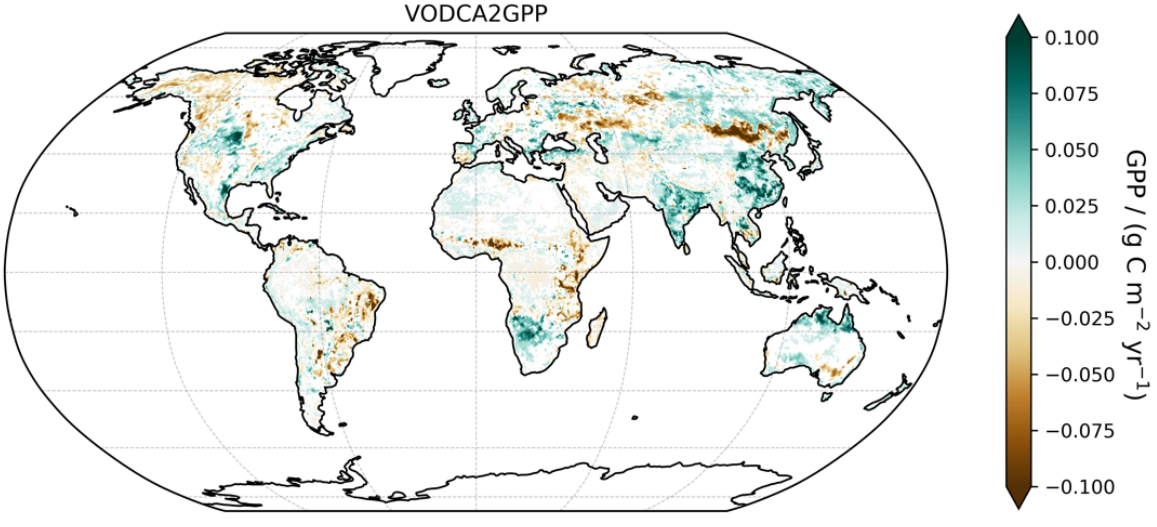

Figure 8: Global map of yearly median GPP trends for the period 1988-2019 for VODCA2GPP. White indicates non-significant trends.

https://doi.org/10.5194/essd-2021-209
Preprint. Discussion started: 24 June 2021

5 Discussion

5.1 Uncertainties in the VODCA2GPP model

The results from the uncertainty analysis and the comparison with in-situ GPP show that VODCA2GPP estimates can be viewed as very reliable across most biomes. However, significant uncertainties were exhibited through the uncertainty analysis in some areas with extreme climatic or topographic conditions (e.g.; deserts and mountain ranges). Also, parts of Eastern and Western Siberia and parts of Southern China show relatively large spreads in the predictions. The observed uncertainty patterns in Siberia might be associated with topography, generally lower data availability (due to frozen masking in VODCA) and a lack of FLUXNET stations. Missing in-situ information might also be a driver for uncertainties in Southern China but the exact cause for the relatively high uncertainty there is unclear. The uncertainty analysis suggests that VODCA2GPP estimates have a tendency to be too high in these regions and thus should be interpreted with caution. Furthermore, moderate uncertainties were also found for the tropics which is likely due to the extremely low in-situ data availability and higher absolute GPP than in mid-latitudes.

The comparison with in-situ GPP shows clear differences in performance of the VODCA2GPP model across different biomes. High performance is achieved in densely vegetated biomes while the performance decreases in arid and less vegetated regions. A reason for the weaker performance in areas with less water availability might be adapted water regulation strategies of plants. Plants in drought-prone regions often reduce transpiration by limiting stomatal conductance in order to maintain a constant water potential even in times of extreme water scarcity (Sade et al., 2012). Since VOD is largely driven by the vegetation's water content, this isohydric behaviour of vegetation could at least partly explain relatively high VOD and consequently also overestimated GPP in those regions (Teubner et al., 2021).

Also, the observation bias which is introduced by unevenly distributed FLUXNET sites decreases the model's robustness. GPP is measured in situ only for few locations where in-situ carbon fluxes are measured and these stations are mostly located in temperate regions (e.g., Europe and North America) while semi-arid and tropical forest regions are underrepresented in the training data.

5.2 Independence of reference datasets

The lack of in-situ GPP is not only problematic in model training but also hampers a fair evaluation and validation on a global scale. Thus, validation in regions with low FLUXNET station density could only be done via global reference datasets. Remote sensing-based references (MODIS and FLUXCOM), however, are also calibrated or trained using in-situ GPP observations (Jung et al., 2020; Running et al., 1999) and can therefore not be viewed as fully independent from VODCA2GPP (Teubner et al., 2021). In contrast to observation-based GPP products, estimates from the TRENDY ensemble can be considered largely independent from VODCA2GPP which makes it a very valuable additional reference for VODCA2GPP.

https://doi.org/10.5194/essd-2021-209
Preprint. Discussion started: 24 June 2021


Open Access Earth System Science Data Discussions

5.3 Limitations in VODCA and their impact on VODCA2GPP

As outlined in Moesinger et al. (2020) there are certain limitations in the VODCA v1 product which are partly also evident in VODCA v2 (Zotta et al., in prep) and thus also propagate to VODCA2GPP. A known issue of VODCA v2 is caused by an observation gap between October 2011 and July 2012 for AMSR-E and AMSR2 (Table 1), which prevents a direct bias removal between the sensors. However, scaling between the sensors is achieved by using TMI observations North/South of 35°N/35S for X and Ku-band. Beyond these latitudes for X- and Ku-band and generally globally for C-band, AMSR-E data from 2010-2012 was matched against AMSR2 data from 2012-2014 under the assumption that trends between 2010-2014 are negligible (Moesinger et al., 2020). The result is that AMSR2 observations exhibit a slight positive bias in parts of North America which is also evident in a spatial break in VODCA v1 X- and Ku-Band trends (Moesinger et al., 2020). Although the impact of this procedure on VODCA2GPP trends is small and spatially limited, users are advised to keep the potential bias in mind when analysing VODCA2GPP data after 2012 for latitudes North/South of 35°N/35°S. Other limitations in VODCA concern the mixing of observations that were retrieved at different geometries (e.g., incidence angles) or observation times (Moesinger et al., 2020) and the data loss in certain regions, mostly in the Himalayas, which is caused by failure of the CDF-matching method due to insufficient input data (Moesinger et al., 2020). These issues, however, only have a small or spatially very limited influence on the final VODCA2GPP product.

5.4 Observed bias between VODCA2GPP and other remote sensing based GPP data

VODCA2GPP compares well with the analysed state-of-the-art remote sensing based products FLUXCOM and MODIS in terms of spatio-temporal patterns. However, in comparison to the GPP datasets driven by optical remote sensing data, VODCA2GPP exhibits higher GPP across most biomes. This positive bias can be partly explained by a reported and observed tendency of FLUXCOM and MODIS to underestimate GPP which is especially pronounced in tropical regions (Turner et al. 2006; Wang et al., 2017; Fig 1; Fig A1). Furthermore, discrepancies in absolute GPP among the products outside the tropics might be caused by assumed overestimation of VODCA2GPP in winter months (i.e., in times with very little or no primary productivity). This overestimation is explicable with the water content in vegetation that is also present in these dormant periods. The sensitivity of microwaves to this water content results in non-zero VOD and, consequently, non-zero GPP (Teubner et al., 2021).

Another potential explanation for overestimation in VODCA2GPP is the presence of surface water and its impact on VOD retrievals. The presence of surface water is known to decrease the brightness temperature of the earth's surface and thus significantly decreases VOD retrievals (Bousquet et al., 2020). The impact of surface water contamination is evident in VODCA pixels that partly contain water bodies (e.g., lakes, rivers). These pixels exhibit systematically lower values than neighbouring pixels without water share. This is on the one hand problematic for the output of the VODCA2GPP model where GPP is presumably systematically underestimated in pixels containing surface water. On the other hand, it also has a non-

https://doi.org/10.5194/essd-2021-209
Preprint. Discussion started: 24 June 2021

negligible effect on model training. This effect is caused by FLUXNET stations located close to water bodies, which hardly impact in-situ GPP retrievals but do cause erroneous VOD-retrievals. As a result, underestimated VOD is trained against unaffected in-situ GPP which causes a slight but systematic global overestimation. A potential solution would be the masking of water-contaminated VOD. However, due to the constraints with temperature in the interaction term (eq. 3.3) this would strongly reduce the data available for training, which would potentially decrease the robustness of the VODCA2GPP model if the number of stations is not generally increased.

5.5 Potential factors for observed trends in VODCA2GPP

There are several potential drivers for long-term increases in GPP, the most important ones being global warming, land-use changes and elevating CO_2 concentrations in the atmosphere (Piao et al., 2019). VODCA2GPP does not show a clear global increase trend in microwave-derived GPP for the period 1988-2019 but does so for the period 2003 and 2015. MODIS GPP also exhibited a slight increase in median global GPP for 2003-2015 but at a slower rate. The strongest increase in global GPP was found for the TRENDY-v7 ensemble for both analysed periods. The observed long-term trends in GPP across the different products supports the theory of elevated atmospheric CO_2 leading to an increased uptake of CO_2 (Haverd et. al, 2020; Walker et al., 2020; Campbell et al., 2017; Schimel et al., 2015). The absence of trends in FLUXCOM is not contradicting this theory as FLUXCOM does not account for CO_2 fertilization effects (Jung et al., 2020). However, an in-situ based trend analysis did not provide enough evidence to prove this hypothesis. Therefore, the global influence of atmospheric CO_2 on vegetation productivity remains uncertain but VODCA2GPP advocates a positive effect of rising CO_2 on GPP.

5.6 Complementarity of VODCA2GPP with existing products

The comparison of spatio-temporal patterns showed that there are many similarities between VODCA2GPP and the reference datasets. The analysis of monthly anomalies exhibited various extreme events in VODCA2GPP that also are found in one or more existing product indicating high plausibility of VODCA2GPP derived anomalies. Furthermore, trends derived from VODCA2GPP contain several plausible patterns that match those derived from the TRENDY-v7 simulations but are not visible in both observational products and vice versa. This suggests that VODCA2GPP has the potential to bridge the gaps between existing observation-based and process-based state-of-the art products and can be used complementary to them.

6 Data Availability

The VODCA2GPP data can be accessed (CC BY-NC-SA 4.0) at TU Data under https://doi.org/10.48436/1k7aj-bdz35 (Wild et al., 2021).

https://doi.org/10.5194/essd-2021-209
Preprint. Discussion started: 24 June 2021

7 Conclusion

In this dataset paper we introduced VODCA2GPP, a long-term GPP data record which uses multi-frequency microwave VODCA and temperature data from ERA5-Land for the upscaling of in-situ GPP from FLUXNET2015. The comparison of VODCA2GPP with FLUXNET in-situ GPP and global state-of-the art GPP datasets showed good correspondence between the products in both the spatial and temporal domain, but with varying performance differences across the biomes. In tropical and arid regions, VODCA2GPP has significantly higher values than the reference datasets. Arid and mountainous areas, were found to have the largest uncertainties. The observed anomalies and trends in VODCA2GPP overall match with anomalies and trends derived from MODIS and Trendy-v7 which is another argument for the validity of VODCA2GPP as well as for increased CO_2 uptake by plants induced by increasing atmospheric CO_2 concentrations. Overall, the analysis showed that the novel microwave remote sensing based VODCA2GPP product is able to complement existing GPP data records.

https://doi.org/10.5194/essd-2021-209
Preprint. Discussion started: 24 June 2021

Open Access Earth System Science Data Discussions

Appendix

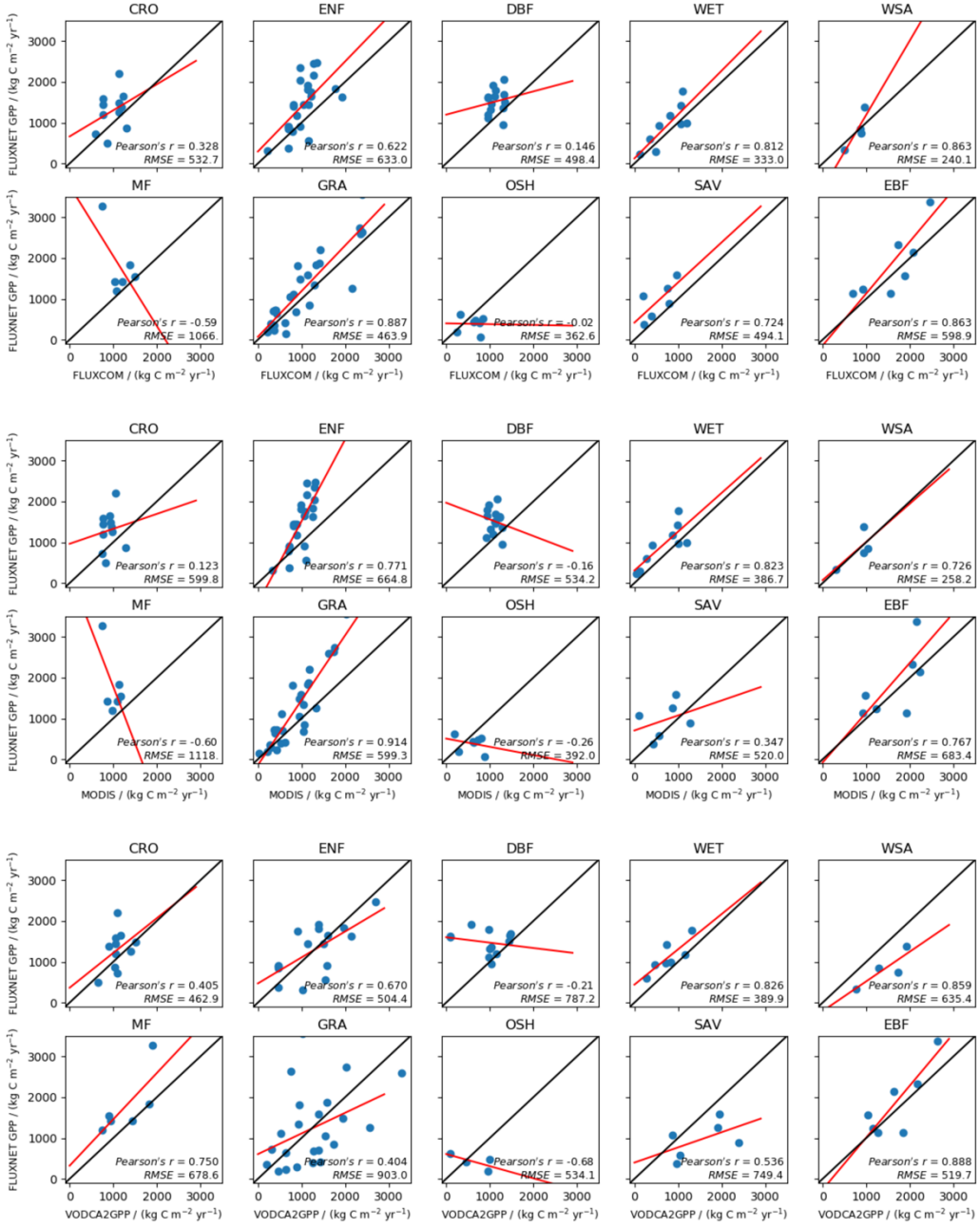

Figure A1: Scatterplots of mean annual GPP for the period 2002-2016 per vegetation type. Vegetation types indicate the predominant IGBP-vegetation type at the respective FLUXNET station.
Abbreviations: CRO: Croplands; ENF: Evergreen Needleleaf Forests; DBF: Deciduous Broadleaf Forests; WET: Permanent Wetlands; WSA: Woody Savannas; MF: Mixed Forests; GRA: Grasslands; OSH: Open Shrublands; SAV: Savannas; EBF: Evergreen Broadleaf Forests

https://doi.org/10.5194/essd-2021-209
Preprint. Discussion started: 24 June 2021

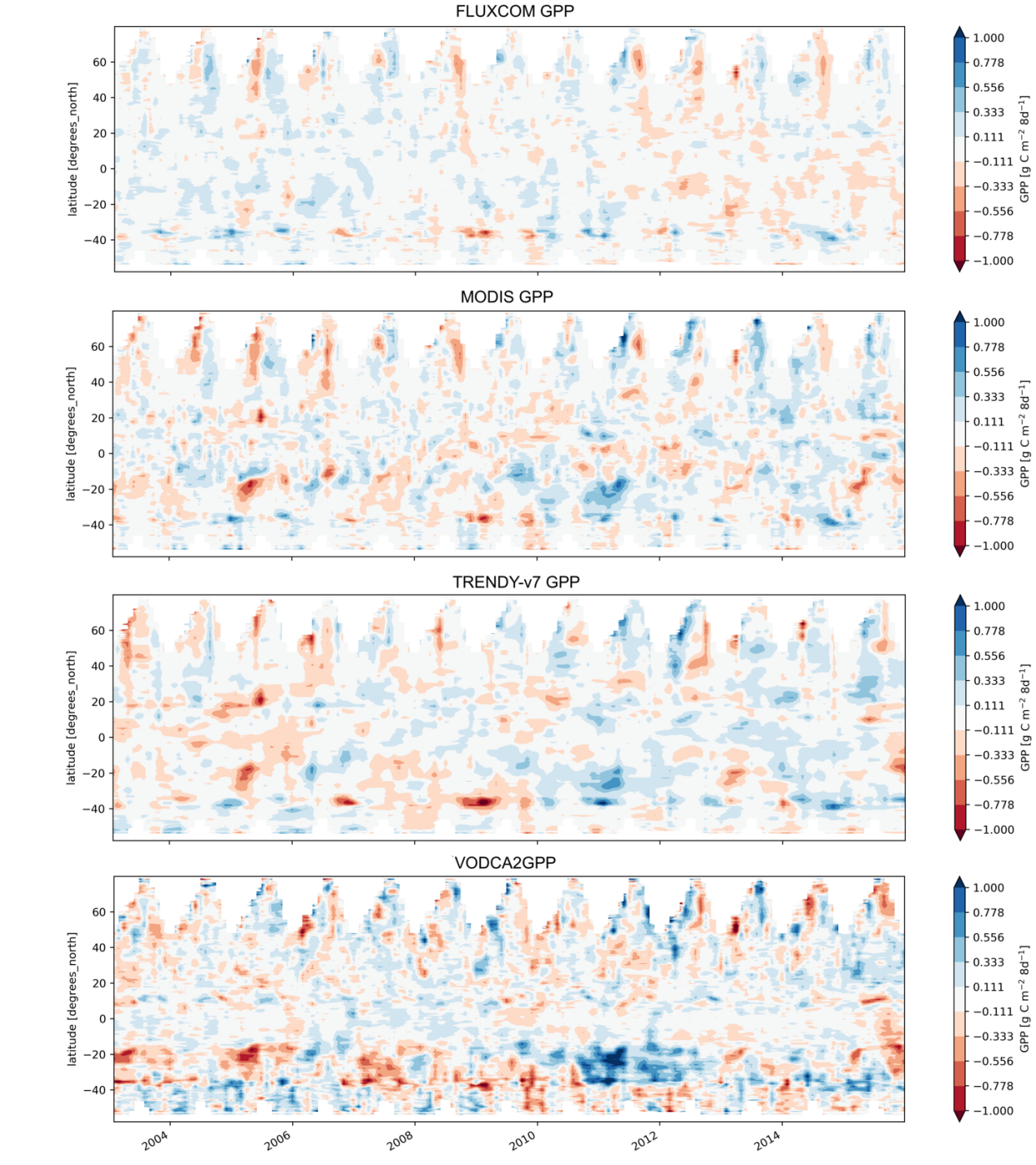

Figure A2: Hovmoeller diagrams of monthly GPP-anomalies for each dataset.

https://doi.org/10.5194/essd-2021-209
Preprint. Discussion started: 24 June 2021

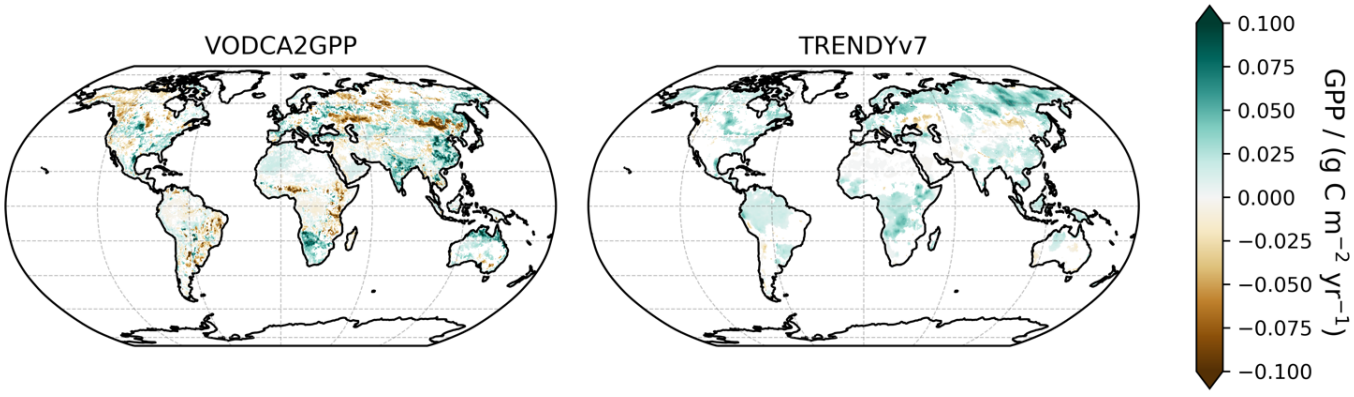

Figure A3: Global maps of yearly median GPP trends for the period 1988-2016 for VODCA2GPP and TRENDY-v7 GPP. White indicates non-significant trends.

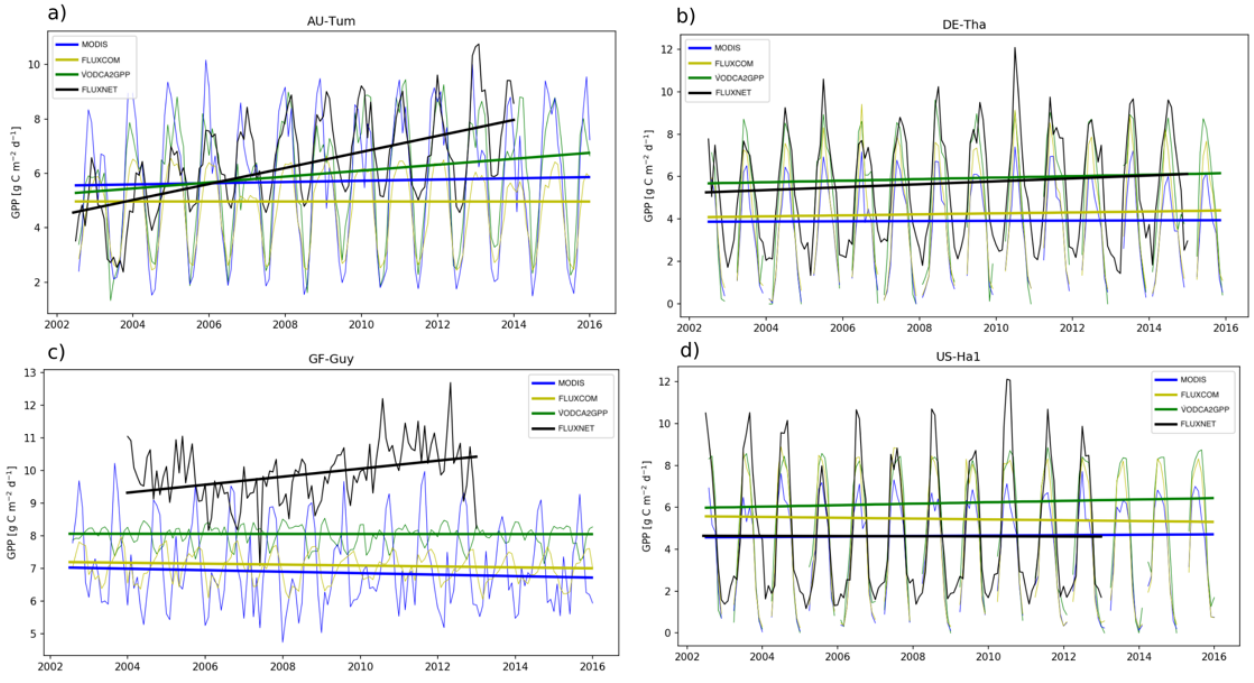

Figure A4 Exemplary collection of time series of in-situ FLUXNET GPP together with extracted time series from MODIS, FLUXCOM and VODCA2GPP. The stations were selected because of their high data availability for the respective landcover. The lines indicate the regression lines as obtained from the Theil-Sen slope estimation. The trends are computed for the common observation period with FLUXNET. The depicted stations are:
a) AU-Tum: Tumbarumba, Australia; Lat: -35.65 °N, Lon: 148.15 °E; Landcover: EBF
b) DE-Tha: Tharandt, Germany; Lat: 50.96 °N, Lon: 13.57 °E; Landcover: ENF
c) GF-Guy: Guyaflux, French Guiana; Lat: 5.28 °N, Lon: -52.93 °E; Landcover: EBF
d)US-Ha1: Harvard Forest EMS Tower, United States; Lat: 42.54 °N, Lon: -72.17 °E; Landcover: DBF

https://doi.org/10.5194/essd-2021-209
Preprint. Discussion started: 24 June 2021

Open Access Earth System Science Data Discussions

Table B1: Overview of FLUXNET Tier1 v1 stations within the period 1991-2014

FLUXNET ID	Name	Lon [°E]	Lat [°N]	Years used
AR-SLu	San Luis	-66.46	-33.46	2009-2011
AR-Vir	Virasoro	-56.19	-28.24	2010-2012
AT-Neu	Neustift	11.32	47.12	2002-2012
AU-ASM	Alice Springs	133.25	-22.28	2010-2013
AU-Ade	Adelaide River	131.12	-13.08	2007-2009
AU-Cpr	Calperum	140.59	-34.00	2010-2013
AU-Cum	Cumberland Plains	150.72	-33.61	2012-2013
AU-DaP	Daly River Savanna	131.32	-14.06	2008-2013
AU-DaS	Daly River Cleared	131.39	-14.16	2008-2013
AU-Dry	Dry River	132.37	-15.26	2008-2013
AU-Emr	Emerald, Queensland, Australia	148.47	-23.86	2011-2013
AU-Fog	Fogg Dam	131.31	-12.55	2006-2008
AU-GWW	Great Western Woodlands, Wester Australia, Australia	120.65	-30.19	2013-2014
AU-RDF	Red Dirt Melon Farm, Northern Territory	132.48	-14.56	2011-2013
AU-Rig	Riggs Creek	145.58	-36.65	2011-2013
AU-Rob	Robson Creek, Queensland, Australia	145.63	-17.12	2014
AU-Tum	Tumbarumba	148.15	-35.66	2001-2013
AU-Whr	Whroo	145.03	-36.67	2011-2013
BE-Bra	Brasschaat	4.52	51.31	2004-2013
BE-Lon	Lonzee	4.75	50.55	2004-2014
BE-Vie	Vielsalm	6.00	50.31	1996-2014
BR-Sa3	Santarem-Km83-Logged Forest	-54.97	-3.02	2000-2004
CA-NS1	UCI-1850 burn site	-98.48	55.88	2001-2005
CA-NS3	UCI-1964 burn site	-98.38	55.91	2001-2005
CA-NS4	UCI-1964 burn site wet	-98.38	55.91	2002-2005
CA-NS5	UCI-1981 burn site	-98.49	55.86	2002-2005
CA-NS6	UCI-1989 burn site	-98.96	55.92	2001-2005
CA-NS7	UCI-1998 burn site	-99.95	56.64	2002-2005
CA-Qfo	Quebec – Eastern Boreal, Mature Black Spruce	-74.34	49.69	2003-2010
CA-SF1	Saskatchewan – Western Boreal, forest burned in 1977	-105.82	54.49	2003-2006
CA-SF2	Saskatchewan – Western Boreal, forest burned in 1989	-105.88	54.25	2001-2005

https://doi.org/10.5194/essd-2021-209
Preprint. Discussion started: 24 June 2021

Continued from previous page

FLUXNET ID	Name	Lon [°E]	Lat [°N]	Year used
CA-SF3	Saskatchewan – Western Boreal, forest burned in 1998	-106.01	54.09	2001-2006
CH-Cha	Chamau	8.41	47.21	2006-2012
CH-Fru	Frübüel	8.54	47.12	2006-2012
CH-Oe1	Oensingen grassland	7.73	47.29	2002-2008
CN-Cha	Changbaishan	128.10	42.40	2004-2005
CN-Cng	Changling	123.51	44.59	2007-2010
CN-Dan	Dangxiong	91.07	30.50	2004-2005
CN-Din	Dinghushan	112.54	23.17	2003-2005
CN-Du2	Duolun_grassland (D01)	116.28	42.05	2006-2008
CN-Ha2	Haibei Shrubland	101.33	37.61	2003-2005
CN-HaM	Haibei Alpine Tibet site	101.18	37.37	2002-2004
CN-Qia	Qianyanzhou	115.06	26.74	2003-2005
CN-Sw2	Siziwang Grazed (SZWG)	111.90	41.79	2010-2012
CZ-BK1	Bily Kriz forest	18.54	49.50	2004-2008
CZ-BK2	Bily Kriz grassland	18.54	49.49	2004-2006
DE-Akn	Anklam	13.68	53.87	2009-2014
DE-Gri	Grillenburg	13.51	50.95	2004-2014
DE-Hai	Hainich	10.45	51.08	2000-2012
DE-Kli	Klingenberg	13.52	50.89	2004-2014
DE-Lkb	Lackenberg	13.30	49.10	2009-2013
DE-Obe	Oberbärenburg	13.72	50.78	2008-2014
DE-RuS	Selhausen Juelich	6.45	50.87	2011-2014
DE-Spw	Spreewald	14.03	51.89	2010-2014
DE-Tha	Tharandt	13.57	50-96	1996-2014
DK-NuF	Nuuk Fen	-51.39	64.13	2008-2014
DK-Sor	Soroe	11.64	55.49	1996-2012
ES-LgS	Laguna Seca	-2.97	37.10	2007-2009
ES-Ln2	Lanjaron-Salvage logging	-3.48	36.97	2009
FI-Hyy	Hyytiala	24.30	61.85	1996-2014
FI-Jok	Jokioinen	23.51	60.90	2000-2003
FR-Gri	Grignon	1.95	48.84	2004-2013

https://doi.org/10.5194/essd-2021-209
Preprint. Discussion started: 24 June 2021

Continued from previous page

FLUXNET ID	Name	Lon [°E]	Lat [°N]	Year used
FR-Pue	Puechabon	3.60	43.74	2000-2013
GF-Guy	Guyaflux (French Guiana)	-52.92	5.28	2004-2012
IT-CA1	Castel d'Asso 1	12.03	42.38	2011-2013
IT-CA2	Castel d'Asso 2	12.03	42.38	2011-2013
IT-CA3	Castel d'Asso 3	12.02	42.38	2011-2013
IT-Cp2	Castelporziano 2	12.36	41.70	2012-2013
IT-Isp	Ispra ABC-IS	8.63	45.81	2013-2014
IT-Lav	Lavarone	11.28	45.96	2003-2012
IT-Noe	Arca di Noé – Le Prigionette	8.15	40.61	2004-2012
IT-PT1	Parco Ticino forest	9.06	45.20	2002-2004
IT-Ren	Renon	11.43	46.59	1998-2013
IT-Ro1	Roccarespampani 1	11.93	42.41	2000-2008
IT-Ro2	Roccarespampani 2	11.92	42.39	2003-2012
IT-SR2	San Rossore 2	10.29	43.73	2013-2014
IT-SRo	San Rossore	10.28	43.73	1999-2012
IT-Tor	Torgnon	7.58	45.84	2008-2013
JP-MBF	Moshiri Birch Forest Site	142.32	44.39	2003-2005
JP-SMF	Seto Mixed Forest Site	137.08	35.26	2002-2006
NL-Hor	Horstermeer	5.07	52.24	2004-2011
NL-Loo	Loobos	5.74	52.17	1996-2013
NO-Adv	Adventdalen	15.92	78.19	2012-2014
RU-Che	Cherski	161.34	68.61	2002-2005
RU-Cok	Chokurdakh	147.49	70.83	2003-2013
RU-Fyo	Fyodorovskoye	32.92	56.46	1998-2013
RU-Ha1	Hakasia steppe	90.00	54.73	2002-2004
SD-Dem	Demokeya	30.48	13.28	2005-2009
US-AR1	ARM USDA UNL OSU Woodward Switchgrass 1	-99.42	36.43	2009-2012
US-AR2	ARM USDA UNL OSU Woodward Switchgrass 2	-99.60	36.64	2009-2012
US-ARM	ARM Southern Great Plains site - Lamont	-97.49	36.61	2003-2012
US-Blo	Blodgett Forest	-120.63	38.90	1997-2007
US-Ha1	Harvard Forest EMS Tower (HFR 1)	-72.17	42.54	1991-2012

https://doi.org/10.5194/essd-2021-209
Preprint. Discussion started: 24 June 2021

Continued from previous page

FLUXNET ID	Name	Lon [°E]	Lat [°N]	Year used
US-Los	Lost Creek	-89.98	46.08	2000-2014
US-MMS	Morgan Monroe State Forest	-86.41	39.32	1999-2014
US-Me6	Metolius Young Pine Burn	-121.61	44.32	2010-2012
US-Myb	Mayberry Wetland	-121.77	38.05	2011-2014
US-Ne1	Mead – irrigated continuous maize site	-96.48	41.17	2001-2013
US-Ne2	Mead – irrigated maize-soybean rotation site	-96.47	41.16	2001-2013
US-Ne3	Mead – rainfed maize-soybean roatation site	-96.44	41.18	2001-2013
US-SRM	Santa Rita Mesquite	-110.87	31.82	2004-2014
US-Syv	Sylvania Wilderness Area	-89.35	46.24	2001-2014
US-Ton	Tonzi Ranch	-120.97	38.43	2001-2014
US-Tw3	Twitchell Alfalfa	-121.65	38.12	2013-2014
US-UMd	UMBS Disturbance	-84.70	45.56	2007-2014
US-Var	Vaira Ranch-Ione	-120.95	38.41	2000-2014
US-WCr	Willow Creek	-90.08	45.81	1999-2014
US-Whs	Walnut Gulch Lucky Hills Shrub	-110.05	31.74	2007-2014
US-Wkg	Walnut Gulch Kendall Grasslands	-109.94	31.74	2004-2014
ZM-Mon	Mongu	23.25	-15.44	2007-2009

Author Contributions

BW curated the dataset, carried out the analysis and drafted the manuscript with inputs from all authors. IT, MF and WD created and designed the model. IT provided the model implementation and contributed to data preparation. LM, RZ and RS produced the VODCA data. SS provided the TRENDY-v7 ensemble data. All authors contributed to discussions about the methods and results and provided feedback and input for the paper.

Competing interests

The authors declare that they have no conflict of interest.

https://doi.org/10.5194/essd-2021-209
Preprint. Discussion started: 24 June 2021

Acknowledgements

Benjamin Wild, Ruxandra-Maria Zotta and Leander Moesinger are supported through the EOWAVE project funded by the TU Wien Wissenschaftspreis 2015, which was awarded to Wouter Dorigo https://climers.geo.tuwien.ac.at/climers/research/vegetation/eowave/. This work used eddy covariance data acquired and shared by the FLUXNET community, including these networks: AmeriFlux, AfriFlux, AsiaFlux, CarboAfrica, CarboEuropeIP, CarboItaly, CarboMont, ChinaFlux, Fluxnet-Canada, GreenGrass, ICOS, KoFlux, LBA, NECC, OzFlux-TERN, TCOS-Siberia, and USCCC. The FLUXNET eddy covariance data processing and harmonization was carried out by the ICOS Ecosystem Thematic Center, AmeriFlux Management Project and Fluxdata project of FLUXNET, with the support of CDIAC, and the OzFlux, ChinaFlux and AsiaFlux offices.

https://doi.org/10.5194/essd-2021-209
Preprint. Discussion started: 24 June 2021

References

Alemohammad, S. H., Fang, B., Konings, A. G., Aires, F., Green, J. K., Kolassa, J., Miralles, D., Prigent, C., and Gentine, P.: Water, Energy, and Carbon with Artificial Neural Networks (WECANN): a statistically based estimate of global surface turbulent fluxes and gross primary productivity using solar-induced fluorescence, Biogeosciences, 14, 4101–4124, https://doi.org/10.5194/bg-14-4101-2017, 2017.

Anav, A., Friedlingstein, P., Beer, C., Ciais, P., Harper, A., Jones,C., Murray-Tortarolo, G., Papale, D., Parazoo, N. C., Peylin, P., Piao, S., Sitch, S., Viovy, N., Wiltshire, A., and Zhao, M.: Spatiotemporal patterns of terrestrial gross primary production: A review, Rev. Geophys., 53, 785–818, doi:10.1002/2015RG000483, 2015.

Atkin, O. and Tjoelker, M.: Thermal acclimation and the dynamic response of plant respiration to temperature, Trends Plant Sci., 8,343–351 ,doi:10.1016/S1360-1385(03)00136-5, 2003.

Baldocchi, D. D.: Assessing the eddy covariance technique for evaluating carbon dioxide exchange rates of ecosystems: past, present and future, Glob. Ch. Biol., 9, 479–492, https://doi.org/10.1046/j.1365-2486.2003.00629.x, 2003.

Baldocchi, D., Ryu, Y., and Keenan, T.: Terrestrial Carbon Cycle Variability, F1000 Research, 5, 2371, https://doi.org/10.12688/f1000research.8962.1, 2016.

Beer, C., Reichstein, M., Tomelleri, E., Ciais, P., Jung, M., Carval-hais, N., Roedenbeck, C., Arain, M. A., Baldocchi, D., Bonan, G.B., Bondeau, A., Cescatti, A., Lasslop, G., Lindroth, A., Lomas,M., Luyssaert, S., Margolis, H., Oleson, K. W., Roupsard, O.,Veenendaal, E., Viovy, N., Williams, C., Woodward, F. I., and Papale, D.: Terrestrial gross carbon dioxide uptake: global dis-tribution and covariation with climate, Science, 329, 834–838, DOI: 10.1126/science.1184984, 2010.

Bonan, G.: Ecological climatology: Concepts and applications, 2ed., Cambridge University Press, Cambridge, UK, New York, 550 pp., 2008.

Bousquet, E., Mialon, A., Rodriguez-Fernandez, N., Prigent, C., Wagner, F. H., and Kerr, Y. H.: Influence of surface water variations on VOD and biomass estimates from passive microwave sensors. Remote Sensing of Environment, 257, ps://doi.org/10.1016/j.rse.2021.112345112345, 2021.

Bureau of Meteorology, Annual Climate Report 2002, URL: http://www.bom.gov.au/climate/annual_sum/2002/index.shtml, Access date: May 10, 2021

https://doi.org/10.5194/essd-2021-209
Preprint. Discussion started: 24 June 2021

Bureau of Meteorology, Annual Climate Report 2003, URL: http://www.bom.gov.au/climate/annual_sum/2003/index.shtml, Access date: May 10, 2021

Bureau of Meteorology, Annual Climate Report 2005, URL: http://www.bom.gov.au/climate/annual_sum/2005/index.shtml, Access date: May 10, 2021

Campbell, J. E., Berry, J. A., Seibt, U., Smith, S. J., Montzka, S. A.,Launois, T., Belviso, S., Bopp, L., and Laine, M.: Large historical growth in global terrestrial gross primary production, Nature, 544, 84–87, , https://doi.org/10.1038/nature22030, 2017

Cox, P. M., Betts, R. A., Jones, C. D., Spall, S. A., and Totterdell, I. J.: Acceleration of global warming due to carbon-cycle feedbacks in a coupled climate model, Nature, 408(6809):184–187, https://doi.org/10.1038/35041539, 2000.

Clark, D. B., Mercado, L. M., Sitch, S., Jones, C. D., Gedney, N.,Best, M. J., Pryor, M., Rooney, G. G., Essery, R. L. H., Blyth, E.,Boucher, O., Harding, R. J., Huntingford, C., and Cox, P. M.: The Joint UK Land Environment Simulator (JULES), model description – Part 2: Carbon fluxes and vegetation dynamics, Geosci.Model Dev., 4, 701–722, doi:10.5194/gmd-4-701-2011, 2011.

De Nijs, A. H. A., Parinussa, R. M., de Jeu, R. A. M., Schellekens, J., and Holmes, T. R. H.: A Methodology to Determine Radio-Frequency Interference in AMSR2 Observations, IEEE T. Geosci. Remote, 53, 5148–5159, https://doi.org/10.1109/TGRS.2015.2417653, 2015.

Drake, J. E., Tjoelker, M. G., Aspinwall, M. J., Reich, P. B., Barton, C. V., Medlyn, B. E., and Duursma, R. A.: Does physiological acclimation to climate warming stabilize the ratio of canopy respiration to photosynthesis?, New Phytol., 211, 850–863, https://doi.org/10.1111/nph.13978, 2016

Frappart, F., Wigneron, J.-P., Li, X., Liu, X., Al-Yaari, A., Fan, L., Wang, M., Moisy,C., Le Masson, E., Lafkih, Z. A., Vallé C., Ygorra, B., and Baghdadi, N.: Global Monitoring of the Vegetation Dynamics from the Vegetation Optical Depth (VOD): A Review. Remote Sens., 12(18):2915, https://doi.org/10.3390/rs12182915, 2020.

Friedlingstein, P., O'Sullivan, M., Jones, M. W., Andrew, R. M., Hauck, J., Olsen, A., Peters, G. P., Peters, W., Pongratz, J., Sitch, S., Le Quéré, C., Canadell, J. G., Ciais, P., Jackson, R. B., Alin, S., Aragão, L. E. O. C., Arneth, A., Arora, V., Bates, N. R., Becker, M., Benoit-Cattin, A., Bittig, H. C., Bopp, L., Bultan, S., Chandra, N., Chevallier, F., Chini, L. P., Evans, W.,

https://doi.org/10.5194/essd-2021-209
Preprint. Discussion started: 24 June 2021

585 Florentie, L., Forster, P. M., Gasser, T., Gehlen, M., Gilfillan, D., Gkritzalis, T., Gregor, L., Gruber, N., Harris, I., Hartung, K., Haverd, V., Houghton, R. A., Ilyina, T., Jain, A. K., Joetzjer, E., Kadono, K., Kato, E., Kitidis, V., Korsbakken, J. I., Landschützer, P., Lefèvre, N., Lenton, A., Lienert, S., Liu, Z., Lombardozzi, D., Marland, G., Metzl, N., Munro, D. R., Nabel, J. E. M. S., Nakaoka, S.-I., Niwa, Y., O'Brien, K., Ono, T., Palmer, P. I., Pierrot, D., Poulter, B., Resplandy, L., Robertson, E., Rödenbeck, C., Schwinger, J., Séférian, R., Skjelvan, I., Smith, A. J. P., Sutton, A. J., Tanhua, T., Tans, P. P., Tian, H., 590 Tilbrook, B., van der Werf, G., Vuichard, N., Walker, A. P., Wanninkhof, R., Watson, A. J., Willis, D., Wiltshire, A. J., Yuan, W., Yue, X., and Zaehle, S.: Global Carbon Budget 2020, Earth Syst. Sci. Data, 12, 3269–3340, https://doi.org/10.5194/essd-12-3269-2020 , 2020.

Gilabert, M. A., Sánchez-Ruiz, S., and Moreno, Á: Annual gross primary production from vegetation indices: A theoretically 595 sound approach, Remote Sensing, 9(3):193, https://doi.org/10.3390/rs9030193, 2017.

Guisan, A., Edwards, T. C., and Hastie, T.: Generalized linear and generalized additive models in studies of species distributions: setting the scene, Ecol. Model., 157, 89–100, 1, https://doi.org/10.1016/S0304-3800(02)00204-1 , 2002.

600 Hastie, T. and Tibshirani, R.: Generalized Additive Models, Vol. 43. CRC press, 1990.

Haverd, V., Smith, B., Canadell, J. G., Cuntz, M., Mikaloff-Fletcher, S., Farquhar, G., Woodgate, W., Briggs, P. R., and Trudinger, C. M. Higher than expected co2 fertilization inferred from leaf to global observations. Glob Change Biol, 26(4):2390–2402, https://doi.org/10.1111/gcb.14950, 2020.

605

Holmes, T. R. H., De Jeu, R. A. M., Owe, M., and Dolman, A. J.: Land surface temperature from Ka band (37 GHz) passive mi-crowave observations, J. Geophys. Res.-Atmos., 114, D04113,doi:10.1029/2008JD010257, 2009.

Horridge, M., Madden, J., and Wittwer, G.: The impact of the 2002–2003 drought on Australia, J. Policy Model., 3, 285–308, 610 https://doi.org/10.1016/j.jpolmod.2005.01.008, 2005.

Jackson, T. and Schmugge, T.: Vegetation effects on the microwave emission of soils. Remote Sen Environ, 36(3):203–212, https://doi.org/10.1016/0034-4257(91)90057-D, 1991.

615 Jung, M., Schwalm, C., Migliavacca, M., Walther, S., Camps-Valls, G., Koirala, S., Anthoni, P., Besnard, S., Bodesheim, P., Carvalhais, N., Chevallier, F., Gans, F., Goll, D. S., Haverd, V., Köhler, P., Ichii, K., Jain, A. K., Liu, J., Lombardozzi, D., Nabel, J. E. M. S., Nelson, J. A., O'Sullivan, M., Pallandt, M., Papale, D., Peters, W., Pongratz, J., Rödenbeck, C., Sitch, S., Tramontana, G., Walker, A., Weber, U., and Reichstein, M.: Scaling carbon fluxes from eddy covariance sites to globe:

https://doi.org/10.5194/essd-2021-209
Preprint. Discussion started: 24 June 2021

synthesis and evaluation of the FLUXCOM approach, Biogeosciences, 17, 1343–1365, https://doi.org/10.5194/bg-17-1343-2020, 2020.

Krinner, G., Viovy, N., de Noblet-Ducoudre, N., Ogee, J., Polcher,J., Friedlingstein, P., Ciais, P., Sitch, S., and Prentice, I. C.:A dynamic global vegetation model for studies of the coupled atmosphere-biosphere system, Global Biogeochem. Cy., 19,Gb1015, doi:10.1029/2003gb002199, 2005.

Le Quéré, C., Andrew, R. M., Friedlingstein, P., Sitch, S., Hauck, J., Pongratz, J., Pickers, P. A., Korsbakken, J. I., Peters, G. P., Canadell, J. G., Arneth, A., Arora, V. K., Barbero, L., Bastos, A., Bopp, L., Chevallier, F., Chini, L. P., Ciais, P., Doney, S. C., Gkritzalis, T., Goll, D. S., Harris, I., Haverd, V., Hoffman, F. M., Hoppema, M., Houghton, R. A., Hurtt, G., Ilyina, T., Jain, A. K., Johannessen, T., Jones, C. D., Kato, E., Keeling, R. F., Goldewijk, K. K., Landschützer, P., Lefèvre, N., Lienert, S., Liu, Z., Lombardozzi, D., Metzl, N., Munro, D. R., Nabel, J. E. M. S., Nakaoka, S., Neill, C., Olsen, A., Ono, T., Patra, P., Peregon, A., Peters, W., Peylin, P., Pfeil, B., Pierrot, D., Poulter, B., Rehder, G., Resplandy, L., Robertson, E., Rocher, M., Rödenbeck, C., Schuster, U., Schwinger, J., Séférian, R., Skjelvan, I., Steinhoff, T., Sutton, A., Tans, P. P., Tian, H., Tilbrook, B., Tubiello, F. N., van der Laan-Luijkx, I. T., van der Werf, G. R., Viovy, N., Walker, A. P., Wiltshire, A. J., Wright, R., Zaehle, S., and Zheng, B.: Global Carbon Budget 2018, Earth Syst. Sci. Data, 10, 2141–2194, https://doi.org/10.5194/essd-10-2141-2018, 2018.

Li, X., Wigneron, J.-P., Frappart, F., Fan, L., Ciais, P., Fensholt, R., Entekhabi, D., Brandt, M., Konings, A. G., Liu, X., Wang, M., Al-Yaari, A., and Moisy, C.: Global-scale assessment and inter-comparison of recently developed/reprocessed microwave satellite vegetation optical depth products, Remote Sens Environ, 253, 112208, https://doi.org/10.1016/j.rse.2020.112208, 2021.

Liu, Y. Y., Van Dijk, A. I., De Jeu, R. A., Canadell, J. G., McCabe, M. F., Evans, J. P., and Wang, G.: Recent reversal in loss of global terrestrial biomass, Nat Clim Change, 5, 470–474, https://doi.org/10.1038/nclimate2581, 2015.

Meesters, A., DeJeu, R., and Owe, M.: Analytical Derivation of the Vegetation Optical Depth From the Microwave Polarization Difference Index, IEEE Geosci. Remote Sens. Lett., 2, 121–123, https://doi.org/10.1109/LGRS.2005.843983, 2005.

Mo, T., Choudhury, B. J., Schmugge, T. J., Wang, J. R., and Jackson, T. J.: A model for microwave emission from vegetation-covered fields, J. Geophys. Res., 87, 11229, https://doi.org/10.1029/JC087iC13p11229, 1982.

Moesinger, L., Dorigo, W., de Jeu, R., van der Schalie, R., Scanlon, T., Teubner, I., and Forkel, M.: The global long-term microwave Vegetation Optical Depth Climate Archive (VODCA), Earth Syst. Sci. Data, 12, 177–196, https://doi.org/10.5194/essd-12-177-2020, 2020.

Monteith, J. L.: Solar radiation and productivity in tropical ecosys-tems, J. Appl. Ecol., 9, 747–766, https://doi.org/10.2307/2401901, 1972.

Muñoz-Sabater, J., Dutra, E., Agustí-Panareda, A., Albergel, C., Arduini, G., Balsamo, G., Boussetta, S., Choulga, M., Harrigan, S., Hersbach, H., Martens, B., Miralles, D. G., Piles, M., Rodríguez-Fernández, N. J., Zsoter, E., Buontempo, C., and Thépaut, J.-N.: ERA5-Land: A state-of-the-art global reanalysis dataset for land applications, Earth Syst. Sci. Data Discuss. [preprint], https://doi.org/10.5194/essd-2021-82, in review, 2021.

Nemani, R. R., Keeling, C. D., Hashimoto, H., Jolly, W. M., Piper, S. C., Tucker, C. J.,Myneni, R. B., and Running, S. W. Climate-driven increases in global terrestrial net primary production from 1982 to 1999. science, 300(5625):1560–1563, https://doi.org/10.1126/science.1082750, 2003.

O'Sullivan, M., Smith, W. K., Sitch, S., Friedlingstein, P., Arora, V. K., Haverd, V., Jain, A., Kato, E., Kautz, M., Lombardozzi, D., Nabel, J, Tian, H., Vuichard, N., Wiltshire, A., Zhu, D., and Buermann, W.:Climate-driven variability and trends in plant productivity over recent decades based on three global products. Global Biogeochem Cy, 34, e2020GB006613. https://doi.org/10.1029/2020GB006613, 2020.

Owe, M., de Jeu, R., and Holmes, T.: Multisensor historical clima- tology of satellite-derived global land surface moisture, J. Geo- phys. Res., 113, F01002, https://doi.org/10.1029/2007JF000769, 2008.

Pastorello, G., Trotta, C., Canfora, E., et al.: The FLUXNET2015dataset and the ONEFlux processing pipeline for eddy covariancedata, Scientific Data, 7, 225, https://doi.org/10.1038/s41597-020-0534-3, 2020.

Piao, S., Wang, X., Park, T., Chen, C., Lian, X., He, Y.,Bjerke, J. W., Chen, A., Ciais, P., Tømmervik, H., Nemani,R. R., and Myneni, R. B.: Characteristics, drivers and feed-backs of global greening, Nat. Rev. Earth Environ., 1, 14–27,https://doi.org/10.1038/s43017-019-0001-x, 2019.

Piles, M., Camps-Valls, G., Chaparro, D., Entekhabi, D., Konings, A. G., and Jagdhuber, T.: Remote sensing of vegetation dynamics in agro-ecosystems using smap vegetation optical depth and optical vegetation indices. Int Geosci Remote Se, pp. 4346-4349, https://doi.org/10.1109/IGARSS.2017.8127964, 2017.

Rodríguez-Fernández, N. J., Mialon, A., Mermoz, S., Bouvet, A., Richaume, P., Al Bitar, A., Al-Yaari, A., Brandt, M., Kaminski, T., Le Toan, T., Kerr, Y. H., and Wigneron, J.-P.: An evaluation of SMOS L-band vegetation optical depth (L-VOD) data sets: high sensitivity of L-VOD to above-ground biomass in Africa, Biogeosciences, 15, 4627–4645, https://doi.org/10.5194/bg-15-4627-2018, 2018.

Running, S. W., Nemani, R., Glassy, J. M., and Thornton, P. E.: MODIS daily photosynthesis (PSN) and annual net primary production (NPP) product (MOD17) Algorithm Theoretical Basis Document, University of Montana, SCF At-Launch Algorithm ATBD Documents (available online at: www.ntsg.umt.edu/modis/ATBD/ATBD_MOD17_v21.pdf), 1999.

Running, S., Mu, Q., and Zhao, M.: MOD17A2H MODIS/terra gross primary productivity 8-day L4 global 500m SIN grid V006, NASA EOSDIS Land Processes DAAC, 2015.

Ryan, M. G., Lavigne, M. B., and Gower, S. T.: Annual carbon cost of autotrophic respiration in boreal forest ecosystems in relation to species and climate, Journal of Geophysical Research: Atmospheres, 102, 28 871–28 883, https://doi.org/10.1029/97JD01236, 1997.

Sade, N., A. Gebremedhin, and M. Moshelion: Risk-taking plants: Anisohydric behavior as a stress-resistance trait. Plant Signal Behav. 7:767-770, https://doi.org/10.4161/psb.20505, 2012

Schimel, D., Stephens, B. B., and Fisher, J. B. Effect of increasing co2 on the terrestrial carbon cycle. P Natl Acad Sci, 112(2):436–441, https://doi.org/10.1073/pnas.1407302112, 2015.

Sen, P. K.: Estimates of the regression coefficient based on Kendall's tau. J Am Stat, 63(324), 1379-1389, 1968.

Servén, D. and Brummitt, C.: pyGAM: generalized additive models in python, Zenodo. DOI, 10, https://doi.org/http://doi.org/10.5281/zenodo.1208723, 2018.

Sitch, S., Friedlingstein, P., Gruber, N., Jones, S. D., Murray-Tortarolo, G., Ahlström, A., Doney, S. C., Graven, H., Heinze, C., Huntingford, C., Levis, S., Levy, P. E., Lomas, M., Poulter, B., Viovy, N., Zaehle, S., Zeng, N., Arneth, A., Bonan, G., Bopp, L., Canadell, J. G., Chevallier, F., Ciais, P., Ellis, R., Gloor, M., Peylin, P., Piao, S. L., Le Quéré, C., Smith, B., Zhu, Z., and Myneni, R.: Recent trends and drivers of regional sources and sinks of carbon dioxide, Biogeosciences, 12, 653–679, https://doi.org/10.5194/bg-12-653-2015, 2015.

https://doi.org/10.5194/essd-2021-209
Preprint. Discussion started: 24 June 2021

720 Taschetto, A. S. and England, M. H.: El Niño Modoki impacts on Australian rainfall, J. Climate, 22, 3167–3174, doi:10.1175/2008JCLI2589.1, 2009.

Teubner, I. E., Forkel, M., Jung, M., Liu, Y. Y., Miralles, D. G., Parinussa, R., van der Schalie, R., Vreugdenhil, M., Schwalm, C. R., Tramontana, G., Camps-Valls, G., and Dorigo, W. A.: Assessing the relationship between microwave vegetation optical
725 depth and gross primary production, Int. J. Appl. Earth Obs., 65, 79–91, https://doi.org/10.1016/j.jag.2017.10.006, 2018.

Teubner, I. E., Forkel, M., Camps-Valls, G., Jung, M., Miralles, D. G., Tramontana, G., van der Schalie, R., Vreugdenhil, M., Mösinger, L., and Dorigo, W. A.: A carbon sink-driven approach to estimate gross primary production from microwave satellite observations, Remote Sens. Environ., 229, 100–113, https://doi.org/10.1016/j.rse.2019.04.022, 2019.
730

Teubner, I. E., Forkel, M., Wild, B., Mösinger, L., and Dorigo, W.: Impact of temperature and water availability on microwave-derived gross primary production, Biogeosciences, 18, 3285–3308, https://doi.org/10.5194/bg-18-3285-2021, 2021.
Theil, H.: A rank-invariant method of linear and polynomial regression analysis. Indagat Math, 12(85), 173, 1950.

735 Tian, F., Brandt, M., Liu, Y. Y., Verger, A., Tagesson, T., Diouf, A. A., Rasmussen,K., Mbow, C., Wang, Y., and Fensholt, R.: Remote sensing of vegetation dynamics in drylands: Evaluating vegetation optical depth (VOD) using AVHRR NDVI and in situ green biomass data over West African Sahel. Remote Sens. Environ., 177, 265–276, https://doi.org/10.1016/j.rse.2016.02.056, 2016.

740 Tjoelker, M., Oleksyn, J., and Reich, P.: Modelling respiration of vegetation: evidence for a general temperature-dependentQ(10), Glob. Change Biol., 7, 223–230,doi:10.1046/j.1365-2486.2001.00397.x, 2001.

Tramontana, G., Jung, M., Schwalm, C. R., Ichii, K., Camps-Valls, G., Ráduly, B., Reichstein, M., Arain, M. A., Cescatti, A., Kiely, G., Merbold, L., Serrano-Ortiz, P., Sickert, S., Wolf, S., and Papale, D.: Predicting carbon dioxide and energy fluxes
745 across global FLUXNET sites with regression algorithms, Biogeosciences, 13, 4291–4313, https://doi.org/10.5194/bg-13-4291-2016, 2016.

Turner, D. P., Ritts, W. D., Cohen, W. B., Gower, S. T., Running,S. W., Zhao M., Costa, M. H., Kirschbaum, A. A., Ham, J. M.,Saleska, S. R., and Ahl, D. E.: Evaluation of MODIS NPP andGPP products across multiple biomes, Remote Sens.
750 Environ.,102, 282–292, https://doi.org/10.1016/j.rse.2006.02.017, 2006.

Van der Schalie, R., de Jeu, R., Kerr, Y., Wigneron, J., Rodríguez- Fernández, N., Al-Yaari, A., Parinussa, R., Mecklenburg, S., and Drusch, M.: The merging of radiative transfer based surface soil moisture data from SMOS and AMSR-E, Remote Sens. Environ., 189, 180–193, https://doi.org/10.1016/J.RSE.2016.11.026, 2017.

Vreugdenhil, M., Dorigo, W. A., Wagner, W., De Jeu, R. A., Hahn, S., and Van Marle,M. J.: Analyzing the Vegetation Parameterization in the TU-Wien ASCAT Soil Moisture Retrieval. IEEE T Geosci Remote, 54(6):3513–3531, https://doi.org/10.1109/TGRS.2016.2519842, 2016.

Walker, A. P., De Kauwe, M. G., Bastos, A., Belmecheri, S., Georgiou, K., Keeling, R., McMahon, S. M., Medlyn, B. E., Moore, D. J. P., Norby, R. J., Zaehle, S., Anderson-Teixeira, K. J., Battipaglia, G., Brienen, R. J. W., Cabugao, K. G., Cailleret, M., Campbell, E., Canadell, J. G., Ciais, P., Craig, M. E., Ellsworth, D. S., Farquhar, G. D., Fatichi, S., Fisher, J. B., Frank, D. C., Graven, H., Gu, L., Haverd, V., Heilman, K., Heimann, M., Hungate, B. A., Iversen, C. M., Joos, F., Jiang, M., Keenan, T. F., Knauer, J., Körner, C., Leshyk, V. O., Leuzinger, S., Liu, Y., MacBean, N., Malhi, Y., McVicar, T. R., Penuelas, J., Pongratz, J., Powell, A. S., Riutta, T., Sabot, M. E. B., Schleucher, J., Sitch, S., Smith, W. K., Sulman, B., Taylor, B., Terrer, C., Torn, M. S., Treseder, K. K., Trugman, A. T., Trumbore, S. E., Mantgem, P. J., Voelker, S. L., Whelan, M. E., and Zuidema, P. A.: Integrating the evidence for a terrestrial carbon sink caused by increasing atmospheric CO2. New Phytologist, 1. https://doi.org/10.1111/nph.16866, 2020.

Wang, L., Zhu, H., Lin, A., Zou, L., Qin, W., and Du, Q.: Evaluation of the Latest MODIS GPP Products across Multiple Biomes Using Global Eddy Covariance Flux Data, Remote Sensing, 9, 5, https://doi.org/10.3390/rs9050418, 2017.

Welp, L. R., Keeling, R. F., Meijer, H. A., Bollenbacher, A. F., Piper, S. C., Yoshimura,K., Francey, R. J., Allison, C. E., and Wahlen, M.: Interannual variability in the oxygen isotopes of atmospheric CO2 driven by El Niño. Nature, 477(7366):579–582, https://doi.org/10.1038/nature10421, 2011.

Wilcox, R. R.: Fundamentals of modern statistical methods: substantially improving power and accuracy, Springer, New York, USA, 34–35, 2010.www.nat-hazards-earth-syst-sci.net/13/3281/2013/Nat. Hazards Earth Syst. Sci., 13, 3281–3289, 2013

Wild, B., Teubner, I., Moesinger, L., Zotta, R. M., Forkel, M., Van der Schalie, R., Sitch, S. and Dorigo, W. A.:VODCA2GPP (Version 1.0.0) [Dataset], Technische Universität Wien, https://doi.org/10.48436/1k7aj-bdz35, 2021.

Wythers, K. R., Reich, P. B., and Bradford, J. B.: Incorporating temperature-sensitive Q10 and foliar respiration acclimation algorithms modifies modeled ecosystem responses to globalchange, J. Geophys. Res. Biogeosci., 118, 77–90, https://doi.org/10.1029/2011JG001897, 2013.

https://doi.org/10.5194/essd-2021-209
Preprint. Discussion started: 24 June 2021

Zhai, P.-M., Yu, R., Guo, Y.-J., Li, Q.-X., Ren, X.-J., Wang, Y.-Q., Xu, W.-H., Liu, Y.-J., and Ding, Y.-H.: The strong El Niño of 2015/16 and its dominant impacts on global and China's climate, J. Meteorol, Res.-P.R.C., 30, 283–297, https://doi.org/10.1007/s13351-016-6101-3, 2016.

Zhao, M., Heinsch, F. A., Nemani, R. R. and Running, S. W.: Improvements of the MODIS terrestrial gross and net primary production global data set. Remote Sens. Environ. 95, 164–176, doi:10.1016/j.rse.2004.12.011, 2005.

Zotta et al., in preparation